

1 Assessment of small-scale variability of rainfall and multi-satellite precipitation estimates  
2 using measurements from a dense rain gauge network in southeast India

3

4 K. Sunilkumar, T. Narayana Rao, S. Satheeshkumar

5 National Atmospheric Research Laboratory, Gadanki

6 Correspondence to: Dr. T. Narayana Rao (tnrao@narl.gov.in)

7 **Abstract**

8 This paper describes the establishment of a dense rain gauge network and small-scale variability  
9 in rain events (both in space and time) over a complex hilly terrain in southeast India. Three  
10 years of high-resolution gauge measurements are used to validate 3-hourly rainfall and sub-daily  
11 variations of four widely used multi-satellite precipitation estimates (MPEs). The network,  
12 established as part of Megha-Tropiques validation program, consists of 36 rain gauges arranged  
13 in a near-square grid area of 50 km x 50 km with an intergauge distance of 6-12 km.  
14 Morphological features of rainfall in two principal rainy seasons (southwest monsoon: SWM and  
15 northeast monsoon: NEM) show marked differences. The NEM rainfall exhibits significant  
16 spatial variability and most of the rainfall is associated with large-scale/long-lived systems  
17 (during wet spells), whereas the contribution from small-scale/short-lived systems is  
18 considerable during the SWM. Rain events with longer duration and copious rainfall are seen  
19 mostly in the western quadrants (a quadrant is 1/4<sup>th</sup> of the study region) in SWM and northern  
20 quadrants in NEM, indicating complex spatial variability within the study region. The diurnal  
21 cycle also exhibits large spatial and seasonal variability with larger diurnal amplitudes at all the  
22 gauge locations (except for 1) during the SWM and smaller and insignificant diurnal amplitudes  
23 at many gauge locations during the NEM. On average, the diurnal amplitudes are a factor 2  
24 larger in SWM than in NEM. The 24-hr harmonic explains about 70% of total variance in SWM

1 and only ~30% in NEM. During the SWM, the rainfall peak is observed between 20 and 02 IST  
2 (Indian Standard Time) and is attributed to the propagating systems from the west coast during  
3 active monsoon spells. Correlograms with different temporal integrations of rainfall data (1, 3,  
4 12, 24 hr) show an increase in the spatial correlation with temporal integration, but the  
5 correlation remains nearly the same after 12 hours of integration in both monsoon seasons. The  
6 1-hr resolution data shows the steepest reduction in correlation with intergauge distance and the  
7 correlation becomes insignificant after ~30 km in both monsoon seasons.

8 Validation of high-resolution rainfall estimates from various MPEs against the gauge rainfall  
9 data indicate that all MPEs underestimate the light and heavy rain. The MPEs exhibit good  
10 detection skills of rain at both 3 and 24 hr resolutions, however, considerable improvement is  
11 observed at 24-hr resolution. Among the different MPEs investigated, Climate Prediction Centre  
12 morphing technique (CMORPH) performs better at 3-hourly resolution in both monsoons. The  
13 performance of Tropical Rainfall Measuring Mission (TRMM) multisatellite precipitation  
14 analysis (TMPA) is much better at daily resolution than at 3 hourly, as evidenced by better  
15 statistical metrics than the other MPEs. All MPEs captured the basic shape of diurnal cycle and  
16 the amplitude quite well, but failed to reproduce the weak/insignificant diurnal cycle in NEM.

17

## 18 **1. Introduction**

19 Precipitation is ranked among the most variable meteorological parameters in the Earth's climate  
20 system. It is also the most important parameter in the water and energy cycles (Levizzani et al.,  
21 2007; Kucera et al., 2013). Understanding and quantification of the variability of precipitation is  
22 important not only for management decisions, but also to unravel the underlying processes  
23 governing the formation of precipitation and its variability. The density of rain gauges in many

1 operational networks is often too poor to capture the small-scale (both in space and time)  
2 variability of rainfall (Habib et al., 2009). Research networks with a high density of gauges, but  
3 covering a limited area, are becoming increasingly popular to understand the sub-grid and sub-  
4 daily scale variability of rainfall. Measurements from such networks are also useful for the  
5 validation of precipitation estimates from microwave radars and imagers (Krajewski et al., 2003;  
6 Habib et al., 2012; Tokay et al., 2014; Dzotsi et al., 2014; Chen et al., 2015). The complexity in  
7 small-scale variability of rainfall increases in hilly terrain (Zangl, 2007; Li et al., 2014). The  
8 rainfall often becomes inhomogeneous due to topographic influence and at times highly  
9 localized, resulting large errors in the retrieved precipitation by passive/active remote sensors  
10 due to non-uniform beam-filling of precipitation within the satellite or radar pixel (Tokay and  
11 Ozturk, 2012). In order to understand the physical processes responsible for such variability,  
12 several studies examined the dependency of rainfall spatial variability (in terms of correlation  
13 distance,  $d_o$ ) on rainfall regimes (Krajewski et al., 2003), seasons, spatial and temporal  
14 aggregation of data (Krajewski et al., 2003; Villarini et al., 2008; Luini and Capsoni, 2012; Chen  
15 et al., 2015; Prat and Nelson 2015), sample size and extreme rain events (Habib et al., 2001) and  
16 geographical features like topography (Li et al., 2014). Proper quantification of spatial  
17 correlation distance mitigates the uncertainty in the upscaling of rainfall from point-to-areal and  
18 also helps in designing rain gauge networks (Bras and Rodriguez-Iturbe, 1993; Villarini et al.,  
19 2008).

20 At present, only a few dense research gauge networks are operational worldwide. Moreover the  
21 gauge locations in operational networks are mostly confined to well-developed and easily  
22 accessible locations. This leaves large spatial data gaps in critically important areas due to the  
23 unavailability of gauges (over open oceans and remote locations). Further, timely dissemination

1 of precipitation data to concerned authorities is another critical issue. Near real-time high-  
2 quality precipitation measurements are vital for several weather and hydrological forecasting  
3 applications, eg., flash flood forecasting and monitoring (Li et al., 2009; Kidd et al., 2009).  
4 Satellite remote sensing is capable of measuring near-real time high-resolution (both in space  
5 and time) precipitation on a global-scale, including oceans and complex terrain, where in-situ  
6 precipitation measurements are missing (Wang et al., 2009). Recently, several merged satellite  
7 products have been developed by effective integration of relatively accurate active and passive  
8 microwave and high-temporal sampling infrared (IR) measurements. These multi-satellite  
9 precipitation estimates (MPEs) are becoming increasingly popular and several such products are  
10 now available providing high-resolution precipitation on near-real time. They include, among  
11 others, Climate Prediction Centre (CPC) morphing technique (CMORPH; Joyce et al., 2004),  
12 TRMM multisatellite precipitation analysis (TMPA; Huffman et al., 2007), Global satellite  
13 mapping of precipitation (GSMaP; Kubota et al., 2007; Aonashi et al., 2009) and Precipitation  
14 estimation from remotely sensed information using artificial neural networks (PERSIANN; Hsu  
15 et al., 1997; Sorooshian et al., 2000) Details of these MPEs, including their spatial and temporal  
16 resolutions and input data used to generate them, are given in Table 1. However, several  
17 sources of uncertainties, including sensor inaccuracies, retrieval algorithms, not fully understood  
18 physical processes and beam-filling factors, limit the accuracy of MPEs (Levizzani et al. 2007).  
19 Therefore, validation of high-resolution MPEs and quantification of their errors are essential  
20 before utilizing them further for operational or research applications. Thus far, a great deal of  
21 effort has been put into evaluate the MPEs in different climatic conditions (Global - Adler et al.,  
22 2001; Turk et al., 2008; Australia, United States of America (USA) and northwestern Europe -  
23 Ebert et al., 2007; Africa and south America - Dinku et al., 2010; India - Prakash et al., 2014;

1 Sunilkumar et al., 2015; Iran - Ghajarnia et al., 2015; China - Chen et al., 2015 and references  
2 therein) and seasons (Tian et al., 2007, Kidd et al., 2012; Sunilkumar et al., 2015). Though  
3 several studies exist on the evaluation of monthly to seasonal rainfall in the literature, only a few  
4 studies focused on validating the rainfall at daily and sub-daily scales (Sapiano and Arkin, 2009;  
5 Sohn et al., 2010; Habib et al., 2012; Kidd et al., 2012; Mehran and Aghakouchak, 2014).

6 The sub-daily evaluation of five MPEs over the USA and Pacific Ocean indicates strong  
7 performance dependence of MPEs on the region and season, i.e., overestimates warm season  
8 rainfall over the USA and underestimates over tropical Pacific Ocean (Sapiano and Arkin, 2009).  
9 They also noted that all MPEs precisely resolved the diurnal cycle of precipitation. Contrary,  
10 Sohn et al. (2010) have noted the underestimation of the amplitude of diurnal cycle by  
11 CMORPH, PERSIANN and National Research Laboratory blended (NRL-blended) precipitation  
12 products over South Korea. The observed biases and random errors are found to be large at  
13 highest resolution (event and hourly scale), but reduce to smaller values when the evaluations are  
14 carried out over the entire study period or when the data are aggregated in space and time (Habib  
15 et al., 2012). The performance evaluation of various MPEs and reanalysis precipitation products  
16 over northwest Europe reveals a strong seasonal cycle in bias, false alarm ratio and probability of  
17 detection (Kidd et al., 2012). A detailed study on the detection capability of intense rainfall by  
18 various MPEs using a dense network of rain gauges reveals that none of the high-resolution (3  
19 hr.) MPEs are ideal for detecting intense precipitation rates (Mehran and AghaKouchak, 2014).

20 The above studies clearly elucidated that the error characteristics obtained for monthly and  
21 seasonal scales may not necessarily be valid for high-temporal resolutions, such as sub-daily  
22 scale and also the performance of MPEs vary in different climatic regions. It is, therefore, highly  
23 essential to perform validation independently at finer temporal scales over different climatic

1 regions. As mentioned above, the evaluation of MPEs for monthly and seasonal monsoon  
2 precipitation was done to some extent over India (Rahman et al., 2009; Uma et al., 2013; Prakash  
3 et al., 2014, Sunilkumar et al., 2015). However, a detailed study on the validation of MPEs at  
4 shorter time scales (sub-daily and daily) does not exist due to the lack of suitable measurements.  
5 Also, there is no detailed documentation on the small-scale variability of precipitation,  
6 discussing the diurnal cycle of precipitation and correlation distance (its dependence on seasons  
7 and temporal aggregation of data). The objectives of this paper, therefore, are to quantify and  
8 understand the small-scale variability (spatial and temporal) of precipitation over a complex hilly  
9 terrain and also to validate high-resolution MPEs using a dense network of rain gauges  
10 established around Gadanki (13.45° N, 79.18° E). This network has been established as part of  
11 Megha-Tropiques (an Indo-French joint satellite mission) validation program (Raju 2013, Roca  
12 et al. 2015). This being the first paper on this network, its establishment and maintenance  
13 (stringent calibration procedures adopted) is also discussed briefly. Although the southwest  
14 monsoon (SWM: June through September) is the main monsoon season for India as a whole, the  
15 southern part of India (including the study region) receives significant amount of rainfall in  
16 northeast monsoon (NEM: October through December; Rao et al., 2009). The final objective of  
17 this paper is, therefore, to understand the seasonal differences in small-scale variability of in-situ  
18 measured rainfall and performance of MPEs.

19 The remainder of this paper is organized as follows: A description of the study region including  
20 topographical features, seasonal differences and prevailing weather conditions is given in section  
21 2. The establishment and maintenance of the rain gauge network is described in section 3. The  
22 morphological characteristics of rain during both monsoon seasons, including the intensity,  
23 duration and small-scale variability are discussed in Section 4. The validation of MPEs at sub-

1 daily and daily scales is performed in Section 5 using a variety of statistical indices. All the  
2 results are summarized in Section 6.

### 3 **2. Description of study region**

4 The rainfall in India exhibits large and complex spatio-temporal variability governed by a variety  
5 of processes, ranging from small-scale convection, orographic lifting and land-sea circulations to  
6 gigantic monsoon system. As mentioned above, the SWM season is primary rainy season when  
7 considered India as a whole, but the southern parts of India receive considerable rainfall during  
8 the NEM (Figures 1a and 1b). The wind pattern (on 850 hPa level shown in Figures 1a and 1b)  
9 also changes dramatically from southwesterlies during SWM to northeasterlies during NEM over  
10 peninsular India. The daily-gridded  $1^\circ \times 1^\circ$  rainfall data generated by India Meteorological  
11 Department (Rajeevan et al., 2006) and European Centre for Medium-Range Weather Forecast  
12 (ECMWF) - Interim (ERA; Dee et al., 2011) have been used to generate the above figures.  
13 Though the conditions in Bay of Bengal, like high seas-surface temperature and cyclonic  
14 circulations, favor the formation of low-pressure systems, they do not intensify to the stage of  
15 cyclone due to the presence of large vertical wind shear during the SWM. These low-pressure  
16 systems and depressions move onto the land along the monsoon trough (a quasi-permanent  
17 trough that extends from the head Bay of Bengal to northwest India, covering north and central  
18 India) and produce copious rainfall in this region. Contrary, the low-pressure systems formed in  
19 the south Bay of Bengal often intensify to cyclonic stage during the NEM. These systems move  
20 northwestward and produce rainfall along the eastern coast and southern parts of India.  
21 The study region is centered around Gadanki, and spreads in an area of 50 km x 50 km in  
22 southeastern India (shown with a box in Figure 1a). The National Atmospheric Research

1 Laboratory (NARL) located at Gadanki is responsible for the establishment and maintenance of  
2 the gauge network. The topography in the study region is complex with hillocks distributed  
3 randomly on a generally east-west sloped surface (Figure 1c). There is a steep gradient in the  
4 north-south direction also due to the Nallamala Hills (highest peak is about 1000 m above sea-  
5 level) in the north of the study region. The coast is nearly 100 km away from the center of the  
6 study region.

7 As seen in Figures 1a and 1b, the rainfall in this region occurs primarily during two monsoon  
8 seasons (SWM and NEM), besides intense thunderstorms in May. While 55% of the annual  
9 rainfall occurs during the SWM, the NEM comprises of 35% of the annual rainfall (Rao et al.,  
10 2009). Remaining 10% occurs during the premonsoon season (March through May). The rain is  
11 predominantly convective during the SWM, whereas the stratiform rain fraction is significant  
12 and comparable to that of convective during the NEM (Saikranthi et al., 2014). The rain during  
13 the SWM occurs primarily due to evening thunderstorms or propagating mesoscale convective  
14 systems (Mohan, 2011). This region is far from the monsoon trough and is generally not under  
15 the influence of monsoon depressions and low-pressure systems that produce copious rainfall in  
16 central and north India (Houze et al., 2007, Saikranthi et al., 2014). However, the cyclones with  
17 varying intensities play a decisive role in altering the spatial distribution of rainfall during the  
18 NEM. During the study period (October 2011- September 2014), 3 cyclones and few  
19 depressions formed in the Bay-of-Bengal and produced copious rainfall in the study region.

### 20 **3. A dense rain gauge network around Gadanki**

21 Dense rain gauge networks are an integral part of validation programs. As part of one such  
22 satellite validation program - Megha-Tropiques (Raju 2013; Roca et al. 2015), NARL has

1 established a dense network of rain gauges in 2011, covering an area of 50 x 50 km<sup>2</sup> centered  
2 around Gadanki. The network consisting of 36 rain gauges spreads from 78.9° E to 79.4° E and  
3 from 13.1° N to 13.6° E (Figure 1c). Rain gauges employed in the present network are of tipping  
4 bucket type with a 20.32 cm diameter orifice, manufactured by Sunrise Technology (Model No.  
5 ST-ARS-2011) . Each tip corresponds to 0.2 mm (or 6.4 ml) rainfall. The gauges are solar-  
6 powered and store high-resolution data at 1-min. resolution at the site on a memory card, which  
7 has the capacity to store 5 years of rainfall data. Additionally, the 1-min. data are transferred in  
8 near real-time about every 30 min. to a server located at NARL using general packet radio  
9 service (GPRS) technology. The acquisition of near real-time data is very useful not only for  
10 research but also to monitor the performance of each gauge. It is possible to reset the gauge, if  
11 required, from the central hub (NARL). Several factors were considered while choosing the  
12 location for rain gauge installation, like its suitability for rain measurement (no obstacle should  
13 be there in a cone of 45°), safety of the instrument, accessibility to the location and coverage of  
14 mobile network (required for data transfer). As a result, the inter-gauge spacing is not uniform,  
15 rather varied from 6 to 12 km, although majority of them are separated by ~ 10 km (Figure 1c).  
16 Although 45° cone for complete azimuth from the rain gauge is ensured, locations with more  
17 clearance in the direction of wind (predominantly east-west in the study region), wherever  
18 possible, have been preferred for the gauge installation.

19 The reliability of the assessment of MPEs depends primarily on the availability of accurate in-  
20 situ ground truth provided by the rain gauge network. Though in-situ gauge measurements  
21 provide better rainfall estimates, they are not error-free. For instance, the systematic errors often  
22 noted in tipping bucket rain gauge measurements are attributed to the winds and its induced  
23 turbulence, wetting of inner walls of the gauge, loss of rain water during the tipping and

1 evaporation of the rain water in the gauge (WMO, 2008). The estimated wind-induced error  
2 through numerical simulations is found to be in the range of 2%-10% for rainfall and increases  
3 with decreasing rain rate and increasing wind speed (Nešpor and Sevruk 1999). The measured  
4 surface winds (at 2 m) in the study area are in general weak and rarely exceed  $4 \text{ m s}^{-1}$  (~2% of  
5 the total data  $> 4 \text{ m s}^{-1}$ ). Therefore, the error due to the wind could be within 5% in our  
6 measurements (Nešpor and Sevruk 1999). The error due to the non-measurement of rain during  
7 tipping can be minimized but not eliminated (WMO, 2008). This error is considerable during  
8 intense rainfall events. To quantify this error, a rain calibrator with 3 high flow rates has been  
9 used (discussed in detail later).

10 The gauge maintenance can be challenging, especially in remote locations and in extreme  
11 weather conditions, for long durations. The rain gauges are carefully calibrated before deploying  
12 in the field. Strict maintenance schedules are adhered, which includes 2 regular visits of a  
13 qualified technician to all the gauges just before the onset of two principal monsoon seasons,  
14 SWM and NEM, (first visit in May and the second in September) and also to malfunctioning  
15 gauges, whenever required, to maintain high-quality data essential for validating high-resolution  
16 MPEs. Three types of checks are performed during each visit, besides monitoring the  
17 performance of sub-systems, time shifts and temporal offsets between gauges (if any, between  
18 the clocks of gauge and a standard laptop) and battery output. 1. To check how well rain gauge  
19 measures the rain amount, known quantity of water sufficient for 5 tips ( $5 \times 6.4 \text{ ml}$ ) is poured  
20 slowly into the rain gauge and compared with the number of tips recorded by the gauge. 2. To  
21 know whether or not each bucket takes the same quantity of rain for tipping, 6.4 ml of water is  
22 poured slowly in each bucket. The problem, if any found, is rectified by adjusting the leveling  
23 screw. This exercise is repeated till both buckets take the same quantity of water for tipping.

1 Nevertheless, such incidents are rare and these kind of adjustments were required 8 times during  
2 three years. 3. To test how well the gauges estimate different intensities of precipitation, a  
3 reference calibrator (Young 52260) with 3 flow rates is employed. The calibrator generates flow  
4 rates of 1000, 1500 and 2000 ml hr<sup>-1</sup>, which corresponds to rain rates of 31.5, 54.3 and 72.6 mm  
5 hr<sup>-1</sup>, respectively, corresponding to a rain gauge with orifice diameter of 20.32 cm (or 8 in.). The  
6 calibrator is filled with water (up to the mark recommended by the manufacturer) and the water  
7 is released into the gauge along the walls of the orifice. By changing the nozzle, the gauge is  
8 allowed to record each flow rate for 5 minutes. The ratios of accumulated rainfall and the  
9 estimated rain rate (from calibrator) for each flow rate are estimated. The ratios are estimated at  
10 each rain gauge station for all 3 flow rates and are shown in Figure 1d. On average, 90% of  
11 gauges show ratio in the range of 0.9 - 1.1 with a mean value nearly equal to 1, indicating that  
12 the gauges are fairly accurate.

#### 13 **4. Small-scale variability of rain**

14 The small-scale variability of rain distribution in a hilly terrain, such as the present study region,  
15 depends on several factors from the horizontal scale of mountains, direction of wind to complex  
16 interactions between flow dynamics and cloud microphysics (Zangl, 2007 and references therein)  
17 besides the differences in large-scale forcing. This section focuses on the small-scale variability  
18 of rain, both in space and time, using 3 years of gauge measurements.

##### 19 **4.1. Morphological features of rain over the study region**

20 To understand the morphological features of rain and also to test how different its pattern from  
21 that of climatology, the spatial distribution of mean seasonal rainfall for SWM and NEM is  
22 examined (Figure 2). The mean is taken over 3 years of seasonal rainfall. The rainfall

1 distribution is somewhat uniform during the SWM, while it shows a large gradient towards  
2 northeast during the NEM. The magnitude of seasonal rain is larger in the SWM (~400 mm)  
3 compared to NEM (200-350 mm). The rainfall during the SWM accounts for 55% of the annual  
4 rainfall, while the NEM contributes 30-35%, consistent with the seasonal rain fractions reported  
5 by Rao et al. (2009). In general, the region along the east coast, particularly close to the southern  
6 tip of India, receives more rainfall during the NEM, the main monsoon season for that region.  
7 However, the rainfall gradually decreases towards west from the East Coast. The present study  
8 clearly shows this gradient in seasonal rainfall with rainfall varying by > 100 mm in just 50 km.  
9 This east-west gradient is not the same at all latitudes, but is larger towards the north. The  
10 highest mountains in the study region lies in that part and are responsible for lifting the moist air  
11 from Bay-of-Bengal reaching that region as part of NEM circulation.

12 The study region receives rainfall due to a variety of processes, starting from small-scale evening  
13 thunderstorms to synoptic-scale cyclones. The rainfall occurred during both monsoon seasons is  
14 considered for the present study, irrespective of its generating mechanism (thunderstorm,  
15 cyclone, etc.). Nevertheless, to know which kind of rain systems (small-scale/short-lived or  
16 large-scale/long-lived) contribute more to total rain amount, the data are segregated into two  
17 groups as small-scale/short-lived and large-scale/long-lived and rain fractions associated with  
18 those systems are estimated at each rain gauge location during both monsoon seasons. The  
19 system is treated as large-scale/long-lived, if rain occurs over more than 75% of the gauge  
20 locations for at least 2 days. Remaining rainfall is treated as associated with small-scale/short-  
21 lived systems. The number of large-scale/long-lived systems and their duration varied from year  
22 to year. On average, the number of large-scale/long-lived systems during the SWM and NEM is  
23 found to be equal, but their average durations differ (6.9 days for SWM and 4.4 days for NEM).

1 The rain fraction due to large-scale/long-lived systems varies considerably (10 - 15%) from year  
2 to year during both the seasons. However, the probability distributions of rain fraction by large-  
3 scale/long-lived systems (not shown here), clearly depicts the seasonal variation. The large-  
4 scale/long-lived systems contribute more to total rain amount during the NEM with  $\frac{3}{4}$  of  
5 locations receive  $>60\%$  of seasonal rain due to these systems. However, same amount of rain  
6 fraction ( $>60\%$ ) by large-scale/long-lived systems is observed only at  $\frac{1}{2}$  of the locations during  
7 the SWM. Though, the number of rainy days associated with large-scale/long-lived systems (due  
8 to longer average duration) is larger during SWM, but their contribution at many of the locations  
9 within the study region is not much. In other words, the small-scale/short-lived systems are also  
10 important during the SWM as they produce considerable fraction of total rain amount.

#### 11 **4.2. Regional variability in rain rate and rain duration**

12 Based on the topography and spatial distribution of rainfall, the study region is roughly divided  
13 into 4 quadrants (Figure 1c). The division appears arbitrary but intuitive. The rain gauge  
14 locations towards the west, i.e., regions 1 and 3, are on elevated land and receive nearly equal  
15 amount of rainfall in both seasons. The locations in region 2 and 4 are on lowland, but the  
16 amount of rainfall that they receive varies considerably during the NEM.

17 To understand the spatial variability within the study region and between the two monsoon  
18 seasons, an event-based analysis is performed. As discussed above, the total study region is  
19 divided into 4 quadrants in such a way that 9 gauges exist in each quadrant. Rain events at each  
20 gauge location within each quadrant are pooled separately for all 4 quadrants. In the present  
21 study, the rain event is defined (for each rain gauge location) as an event with a rain duration  $> 5$   
22 min. and an accumulated rain exceeding 0.5 mm. Further, the temporal gap between any two rain

1 events should not be less than 25 minutes. If rain occurs again within 25 minutes after the first  
2 shower, then it is considered as part of the first shower. The 25 min. threshold is chosen as the  
3 gauge takes nearly 25 min. for one tip in the presence of drizzle, at  $0.5 \text{ mm hr}^{-1}$  (assuming rain is  
4 continuous and evaporation is negligible). Rain duration and accumulations are estimated from  
5 these rain events and their cumulative distributions are shown in Figure 3. Rain event statistics  
6 (of event duration and accumulated rainfall) for each quadrant, like mean, maximum and  
7 interquartile range (IQR: 75%-25%) and 90th percentile, are presented in Table 2. The 90<sup>th</sup>  
8 percentile is considered for representing the extreme rainfall events. The above statistics are  
9 presented for both SWM and NEM to delineate the seasonal differences, if any exist.

10 During both monsoons, the number of rain events is sufficiently large ( $> 500$ ) in each quadrant  
11 for obtaining robust statistics. The number of events is largest in the 2<sup>nd</sup> quadrant in both  
12 monsoons, a quadrant in which most of the gauges are located near the foot hills of relatively  
13 high mountains, suggesting possible influence of mountain flows in enhancing cloud activity in  
14 this quadrant. In general, more rain events are observed during the SWM than in NEM in all  
15 quadrants. The SWM is a summer monsoon and most of the rainfall in this season is associated  
16 with evening convection due to intense heating, mesoscale flows (convection due to mountain  
17 and sea-breeze circulations)(Simpson et al., 2007) and propagating systems (Mohan, 2011)  
18 (discussed in detail later). Many of them are short-lived as can be evidenced from their  
19 cumulative distributions (Figure 3). For example, 50% of the events during the SWM have  
20 durations  $< 35$  min. compared to  $\geq 40$  min. in NEM in all quadrants.

21 A sensitivity analysis has been performed (not shown here) to understand the impact of  
22 thresholds used in the present study (25 min. for separating rain events and a rain rate  $< 0.5$   
23 mm/event for omitting the events from the analysis) on distributions for event duration and rain

1 rate (mm/event). Three years (October 2011- September 2014) of impact-type disdrometer data  
2 collected at NARL, Gadanki have been used as it provides 1-min. rain rates (Rao et al. 2001).  
3 The distributions for event duration and rain rate have been generated by employing three  
4 different temporal intervals for separating rain events, 25, 60 and 120 minutes. As expected, the  
5 distributions for rain duration shifted to longer durations with the increase in time for shower  
6 separation. Nevertheless, the rain rate distribution remained nearly the same. The impact of  
7 omission of data with rain rates  $< 0.5$  mm/event is also found to be negligible.

8 During the SWM, the statistics of rain events in two western quadrants are different from that of  
9 eastern quadrants. It is clear from Figure 3a and Table 2 that both duration of the event and rain  
10 accumulation within the event are larger in quadrants 1 and 3 than in 2 and 4. The difference is  
11 quite pronounced in the case of extreme rainfall events (i.e., 90<sup>th</sup> percentile). Over the study  
12 region, the long lasting events that produce copious rainfall generally occur during the late night  
13 - midnight period during active monsoon spells. Mohan (2011), using Hovmöller diagram of 3-  
14 hourly TMPA rainfall, has shown that these long-lasting rain bands are propagating systems  
15 from the west coast. These systems start propagating from the west coast in the evening and reach  
16 the study region, which is nearly 400 km from the west coast (see Figure 1a), around the mid-  
17 night. Inspection of background meteorological parameters like low-level wind shear and  
18 convective available potential energy (CAPE) reveals that the propagation could be associated  
19 with wind shear-cold pool interaction on the down shear regime (Weisman and Rotunno 2004).  
20 The intensity of propagating systems gradually diminishes as they move from the west to east.  
21 At times, these propagating systems produce rainfall over the gauge locations in the western  
22 quadrants, but not in eastern quadrants because the rain bands dissipate before reaching the  
23 eastern quadrants. This is depicted in pictorial form in Figures 4a and 4b for SWM and NEM,

1 respectively, showing the event duration and rain accumulation as a function of local hour in all  
2 quadrants. The number, duration and rain accumulation of events during 19 - 04 IST (Indian  
3 standard time) in the western quadrants exceeds those in eastern quadrants. Also, events with  
4 longer duration and greater rain accumulation are almost absent during the morning-noon period  
5 (08-12 IST) in the western quadrants, while a few such events exist in the eastern quadrants. It is  
6 strikingly apparent from Figure 4a that there is a clear diurnal pattern in event duration in all 4  
7 quadrants, though the pattern appears to be smeared in the eastern quadrants. The eastern  
8 quadrants, being relatively closer to the coast, may sometimes get rain due to sea-breeze  
9 intrusions (Simpson et al., 2007). This coupled with the inability of some propagating systems to  
10 reach these quadrants appear to be the reasons for a different diurnal pattern.

11 Significant regional variability is also observed in rain duration and accumulation during the  
12 NEM, wherein the northern quadrants (numbered 1 and 2) experience long lasting events with  
13 more rainfall than their counterparts in the southern quadrants (numbered 3 and 4) (Figures 3b  
14 and 4b). Almost all the long-lasting events in northern quadrants (1 and 2) produced significant  
15 amount of rainfall ( $> 20$  mm), while it is not the case in southern quadrants. The north-south  
16 regional differences are distinctly apparent in extreme rainfall cases also (90<sup>th</sup> percentile) (Table  
17 2). Events with longest duration and highest rainfall, on the other hand, are seen in the eastern  
18 quadrants. For example, the 4<sup>th</sup> quadrant has 6 events with longer than 10 hours duration with  
19 one event producing rainfall continuously for nearly one day (1425 min). This event is associated  
20 with a cyclone, 'Neelam', that passed close (~50 km south of Gadanki) to the observational site  
21 on 31 November 2012. In fact, this cyclone has produced steady rainfall over several rain gauge  
22 locations leading to long-lasting events (16 events with duration longer than 6 hours are observed  
23 during the passage of Neelam). This number increased to 53, when events with 3 hours or longer

1 are considered. The observed IQR for rain duration also shows a different pattern during the  
2 NEM, where the values in all quadrants are not significantly different from each other. In  
3 contrast to the clear diurnal pattern in rain events and duration during the SWM, the NEM does  
4 not show any clear signature of diurnal pattern.

### 5 **4.3. Diurnal variability**

6 Figure 4 clearly demonstrated the diurnal pattern in number of events and duration in both the  
7 monsoon seasons. This section further discusses the spatial and seasonal variability in the diurnal  
8 cycle of rainfall. The diurnal variation is the fundamental mode of variability in the precipitation  
9 time series and the time of occurrence of maximum rainfall depends on several factors, like the  
10 underlying surface (land or ocean), mesoscale circulations, topography, etc. (Nesbitt and Zipser,  
11 2003, Janowiak et al., 2005; Yang and Smith, 2006; Kikuchi and Wang, 2008). Since the study  
12 region is located in a complex hilly terrain and is about 75-125 km from the coast, several  
13 mesoscale circulations triggered by topography and land-sea contrast, besides the propagating  
14 systems could alter the rainfall pattern. To better understand these processes during SWM and  
15 NEM, the diurnal variation of rainfall at each location has been studied during the two monsoon  
16 seasons.

17 The mean hourly rainfall (hourly accumulated rainfall from all the days in a season/number of  
18 days) time series at each gauge location is subjected to harmonic analysis. The amplitude and  
19 phase of the diurnal cycle, thus obtained, at each location is depicted in Figure 5 for both SWM  
20 and NEM. The arrow magnitude and direction represent the amplitude and phase (time of  
21 maximum rainfall in the form of a 24 hr. clock) of the diurnal cycle, respectively. For instance,  
22 the arrow pointing up ( $0^\circ$ ), right ( $90^\circ$ ), down ( $180^\circ$ ) and left ( $270^\circ$ ) denote, respectively, the

1 rainfall maxima at 00, 06, 12 and 18 IST. The statistical significance of the amplitude is  
2 evaluated by using the F-statistic (Anderson, 1971). Statistically insignificant amplitudes are  
3 shown with blue arrows. The topography is also shown in the figure (shading) for easy  
4 visualization of mountain effects, if any, on the diurnal cycle.

5 Clearly, the rainfall shows distinctly different diurnal cycles during SWM and NEM. Except for  
6 one location, the diurnal cycle is significant with large amplitudes at all locations during the  
7 SWM. Though the diurnal cycle is insignificant at one location (station numbered 10), the  
8 seasonal rainfall at this location doesn't show any anomalous behavior (the seasonal rainfall at  
9 this location is nearly equal to that of its surrounding locations). On the other hand, the diurnal  
10 cycle is insignificant at several locations (15) during the NEM. Even those locations at which  
11 the diurnal variation is significant, the amplitudes are smaller than those observed during SWM.  
12 For instance, during the SWM, 17 locations show diurnal amplitudes larger than the largest  
13 diurnal amplitude in NEM. On average, the diurnal amplitudes are larger by a factor of ~ 2 in  
14 SWM than in NEM.

15 The diurnal cycle also exhibits spatial variability during both monsoon seasons. The diurnal  
16 cycle is stronger in western quadrants of the study region during the SWM, as evidenced by the  
17 large diurnal amplitudes. Though several rain events occur during the afternoon - evening period  
18 (~40% of total events occur during 14 - 19 IST), most of them are short-lived and contribute only  
19 30% to the seasonal rainfall. On the other hand, 50% of total events occur during 20 - 00 IST, but  
20 they occupy ~60% of seasonal rain amount (Figure 4). Among 4 quadrants, the rain fraction by  
21 events occurring during 20-00 IST is highest in western quadrants (1 and 3, wherein it exceeds  
22 62 - 67%). The diurnal cycle shows a broad peak during 20 - 00 IST at all the locations with  
23 maxima at 21 IST. One would expect an evening peak in the diurnal cycle of rainfall over the

1 land, when the convective instability induced by solar heating increases, resulting cloud  
2 formation and precipitation. However, the diurnal cycle in rainfall in the study region peaks  
3 much later and this peak is primarily associated with the propagating systems (Mohan, 2011).  
4 During the NEM, except for 6 locations that show an evening peak (16-18 IST) in the diurnal  
5 cycle, all other locations (30) depict a broad peak during 18 - 22 IST. In this season, the rainfall  
6 is governed by a variety of processes, like depressions/cyclones originated in adjoining Bay-of-  
7 Bengal, small-scale evening thunderstorms, advection of nocturnal precipitating systems from  
8 Bay-of-Bengal, mountain-induced rainfall (either by lifting the moist air reaching the study  
9 region with the synoptic flow or by generating convergence zones for convection during the  
10 night). These processes generate rainfall that either doesn't show any diurnal cycle (like  
11 cyclones) or peaks at different timings (solar heating-induced convection peaks during the  
12 evening, rainfall due to advection from Bay-of-Bengal in the morning, mountain-induced rainfall  
13 during the night), producing a weaker (in some cases insignificant) diurnal cycle of rainfall. The  
14 spatial variability in the diurnal cycle is also considerable with majority of the locations in the  
15 eastern quadrants showing significant diurnal cycle. Contrary, the diurnal cycle is insignificant  
16 at several locations in the western quadrants.

17 The present study mainly focuses only on the first harmonic (24 hr. component) of the diurnal  
18 variation, as it is regarded as the dominant mode by earlier studies elsewhere. To examine this  
19 issue and also to quantify how much variance the 24-hr component explains in the total variance,  
20 both total variance and variance due to 24-hr harmonic are estimated. Figure 5c shows the  
21 contribution of 24-hr harmonic to the total variance at each rain gauge location during SWM and  
22 NEM seasons. It is clearly evident from Figure 5c that the 24-hr component is the dominant  
23 mode in the diurnal variation of rainfall during the SWM. It explains 40-90% of the total

1 variance of the diurnal cycle at different locations with an average contribution of ~70%. Only  
2 one station (No. 10), where the diurnal cycle is insignificant (Figure 5a), shows less contribution  
3 to the diurnal variance. On the other hand, the contribution of 24-hr harmonic to the total  
4 variance is mere ~30% (on average) during the NEM, indicating that other high frequency modes  
5 might be important during the NEM. Also, the diurnal component contributes < 20% to the total  
6 variance at several locations (1/3 of total number of locations). As discussed above, several  
7 processes including the evening convection, early morning rain due to oceanic clouds, wide  
8 spread and continuous cyclonic rain weaken the diurnal cycle during the NEM.

#### 9 **4.4 Spatial correlation**

10 To understand the similarities and differences in spatial coherence of rainfall between the two  
11 monsoon seasons, correlation analysis is performed. Earlier studies have shown the usefulness  
12 of such analysis in gauge-satellite comparisons, hydrological and meteorological modelling and  
13 setting-up gauge networks (Habib et al., 2001; Krajewski et al., 2003; Ciach and Krajewski,  
14 2006; Villarini et al., 2008; Liechti et al., 2012; Luini and Capsoni, 2012; Mandapaka and Qin,  
15 2013, Li et al., 2014, Chen et al., 2015). Spearman correlation coefficients have been computed  
16 between each pair of rain gauge locations for different rain accumulation periods. In the present  
17 study, 4 accumulation periods are considered (1, 3, 12 and 24 hr.) to understand the spatial  
18 correlation structure on varying rain accumulation periods (temporal scales).

19 The spatial correlation of rainfall between different rain gauge locations at different rain  
20 accumulation periods (1, 3, 12 and 24 hr.) is plotted as a function of gauge distance in Figure 6 (a  
21 for SWM and b for NEM). The spatial correlation distance is obtained by fitting a modified

1 exponential model on the data samples in correlograms (intergauge correlation coefficient vs.  
2 intergauge distance), as given by Ciach and Krajewski (2006),

$$3 \quad \rho(d) = \rho_0 \exp \left[ - \left( d/d_0 \right)^{s_0} \right] \quad (1)$$

4 where  $\rho_0$  is the nugget parameter signifying the local decorrelation (caused by random  
5 instrumental errors),  $d$  is the distance between the pair of gauges (varies from 6 to 73.5 km in the  
6 present study),  $d_0$  is the correlation distance (or scale parameter) and  $s_0$  is the shape parameter.

7 The integration time,  $d_0$  and  $s_0$  are also depicted on the figure for ease of comparison.

8 It is clearly evident from Figure 6 that the correlation decreases with increasing gauge distance  
9 and increases with the accumulation time, consistent with earlier studies (Krajewski et al., 2003;  
10 Villarini et al., 2008; Luini and Capsoni, 2012; Li et al., 2014). The steepest decrease of  
11 correlation is observed with 1 hr. integrated rain, which shows insignificant correlation (<0.2)  
12 after ~30 km. Further, the spatial correlation (in terms of correlation distance and slope) varies  
13 rapidly with time scales up to 3 hours, but remains nearly the same for rain accumulations of 12  
14 and 24 hr. The correlograms for all rain accumulations show large scatter around the model  
15 curve even at shorter gauge distances. The large scatter indicates that the rainfall in the study  
16 region is quite variable both in space and time. Because of this large variability even at shorter  
17 distances, the nugget parameter shows values in the range of 0.8-0.95 (for different  
18 accumulations). These features are observed during both monsoon seasons, albeit with differing  
19 slopes and correlation distances. The correlation characteristics exhibit some seasonal variation  
20 for all rain accumulations, as evidenced by different correlation distance and slope values during  
21 SWM and NEM. The correlation distances (slope) during the NEM are found to be larger than  
22 in SWM, indicating higher spatial correlation of rainfall during NEM. The observation of

1 weaker correlation during SWM than in NEM is consistent and analogous to earlier reports that  
2 show smaller correlation distances during summer than in winter (Baigorria et al., 2007; Dzotsi  
3 et al., 2014; Li et al., 2014). Weak correlation in summer is attributed to the large spatial  
4 variability of rainfall due to highly localized and short-lived convective systems (Krajewski et  
5 al., 2003; Dzotsi et al., 2014; Li et al., 2014). It indeed is true that such systems occur frequently  
6 during the SWM over the study region (Figures 3 and 4).

## 7 **5. Validation of high-resolution MPEs**

8 As mentioned in Section 1, several evaluation studies exist in the literature focusing on the  
9 assessment of seasonal rainfall over India (Uma et al., 2013; Prakash et al., 2014; Sunilkumar et  
10 al., 2015), but none of them dealt with high-resolution (temporal) measurements. This aspect has  
11 been studied in detail in this section, in which the focus is primarily on the validation of high-  
12 resolution MPEs using a variety of metrics and statistical distributions and also on the diurnal  
13 cycle of rainfall. As seen in Table 1, MPEs provide precipitation information with different  
14 temporal and spatial resolutions. For proper assessment of MPEs, they need to be uniform and  
15 should match with the reference. First, all MPEs are temporally integrated for 3 hours and then  
16 remapped onto  $0.25^\circ \times 0.25^\circ$ . The study region, therefore, will have 4 satellite grid points.  
17 Among them, one grid point is chosen (for the validation) ( $13.375^\circ$  N,  $79.125^\circ$  E) in such a way  
18 that the grid point is close to the center of the network and the rainfall and terrain are somewhat  
19 homogeneous around that grid (dashed box covering a region of  $0.25^\circ \times 0.25^\circ$  in Figure 1c).  
20 Moreover, the diurnal cycle at all locations (9 in number) within the selected region is somewhat  
21 similar. The intergauge spacing within the selected region is in the range of 6-12 km, which is  
22 much smaller than  $d_0$  of 3-hourly rainfall in this area (Figure 6). It is known from earlier studies  
23 that the density of operational gauges is often too small to resolve the rainfall variations at

1 smaller scales (Habib et al. 2009). However, the 6-12 km intergauge distance employed here is  
2 almost equal to the highest resolution given by MPEs (i.e., 8 km by CMORPH) and therefore  
3 they can serve as a reference for validating high-resolution MPEs. However, to match the  
4 resolution of other MPEs ( $0.25^\circ \times 0.25^\circ$ ), the rainfall data at the selected grid is obtained by  
5 interpolating (using inverse distance weighting) the data at all the locations within the selected  
6 region. Further, to discard the rain data arising due to the gridding, a rain threshold of 0.5 mm  
7 per 3 hr. is used as a lower threshold to discriminate the rain from no rain.

8 The validation of rain rates generated by MPEs is performed in a statistical way by comparing  
9 the cumulative distributions of 3-hr rain rates by MPEs with rain gauge network (Figure 7). Note  
10 that the frequency bins of cumulative distribution are taken for logarithmic values of 3-hr rain  
11 rates. Figure 7 clearly shows that all MPEs severely underestimate the drizzle rain having rain  
12 rates less than  $0.8 \text{ mm } 3\text{hr}^{-1}$ . Although the underestimation at low rain rates is seen during both  
13 monsoon seasons, it is severe in NEM. Later it will be shown that this underestimation is partly  
14 due to MPEs inability to detect the light rain and partly due to the underestimation of rain rates in  
15 light rain (to values  $< 0.5 \text{ mm } 3\text{hr}^{-1}$ , the threshold used to detect the rain). Among different data  
16 sets, the underestimation is severe in the case of TMPA, but is less in PERSIANN. While the  
17 distributions for MPEs and reference show a very good agreement for rain rates  $1 - 8 \text{ mm } 3\text{hr}^{-1}$ ,  
18 but all MPEs overestimate rain rates during the moderate-heavy rain ( $8 - 20 \text{ mm } 3\text{hr}^{-1}$ ). The  
19 PERSIANN hardly shows rain rates greater than  $25 \text{ mm } 3\text{hr}^{-1}$ . Nevertheless, the number of  
20 samples in higher rain rate bins is quite small and need to be dealt carefully.

21 All MPEs are validated for their detection capabilities and also for quantifying the root mean  
22 square error (RMSE) at two temporal resolutions (3-hr and 24-hr). While 3-hr corresponds to the  
23 highest temporal resolution that most of MPEs provide, the 24-hr rain accumulation is the

1 commonly used temporal integration in such evaluation studies (Ebert et al., 2007; Habib et al.,  
2 2012; Sunilkumar et al., 2015 and references therein). Table 3 shows validation statistics in  
3 terms of detection metrics (in %) (Probability of detection (POD- both reference and MPEs  
4 detect the rain correctly), false alarm ratio (FAR- MPEs detect the rain wrongly), misses  
5 (missing rain- MPEs fail to detect the rain)), and accuracy metrics (correlation coefficient and  
6 RMSE; Ebert et al., 2007; Sunilkumar et al., 2015 for formulae). The detection metrics clearly  
7 show marked differences between the seasons and also between MPEs within the season. All  
8 MPEs exhibit good detection skills of rain at 3- and 24-hr temporal resolutions, however, the 24-  
9 hr accumulation provides relatively better statistics (higher POD during both seasons). Although  
10 the detection skills of all MPEs improve with higher temporal accumulation, the degree of  
11 improvement varied from season to season and also between different data sets. It varied by ~20-  
12 65% during the SWM, but the improvement is only marginal for 3 data sets during NEM (<20%,  
13 but only TMPA shows considerable improvement in POD with longer rain accumulation).

14 The FAR values validated at 3-hr accumulation are quite small and show large seasonal  
15 differences. Examination of data reveals that these small values are due to the large number of  
16 non-rainy data points in the reference data (it appears in the denominator). Nevertheless, the  
17 FAR values increase with temporal accumulation and are nearly comparable with those available  
18 in the literature (Sunilkumar et al., 2015). The study region being a semi-arid region with dry  
19 atmospheric conditions, evaporation of falling rain is found to be significant with higher fraction  
20 of virga rain (predominant during SWM) (Radhakrishna et al. 2008; Saikranthi et al., 2014).  
21 Since MPEs depend mostly on cloud top temperature or ice scattering signature for deriving  
22 rainfall over the land, significant evaporation of falling rain and higher fraction of virga rain  
23 results larger FAR values (Sunilkumar et al., 2015). For the same reason, the missing rain is

1 expected to be less. Contrary, the missing rain is found to be quite high in both monsoon seasons,  
2 particularly with 3-hr rain accumulation data. Although with 24-hr accumulation, the fraction of  
3 missing rain reduced considerably during the SWM, but not in NEM. Interestingly, the observed  
4 percentage of missing rain is comparable to that obtained by Sunilkumar et al. (2015) using an  
5 independent data set as the reference ( $1^\circ \times 1^\circ$  gridded operational rainfall data set). The reasons  
6 for higher fraction of missing rain during NEM even with longer time integration are not  
7 immediately obvious. Several possibilities exist for the observed large fraction of missing rain  
8 during NEM, like higher occurrence of weaker rain, the underestimation of weak rain (0.5-1 mm  
9  $3\text{hr}^{-1}$ ) by MPEs, higher occurrence of shallow rain. The data are examined for the existence of  
10 such instances in both the seasons. The occurrence percentage of weak rain with rain rates 0.5-1  
11 mm  $3\text{hr}^{-1}$  is found to be high (~35%) and nearly equal in both monsoon seasons, indicating that it  
12 may not be the real cause. The second aspect, the underestimation of rain rates by MPEs, could  
13 be a decisive factor, particularly in the presence of considerable fraction of weaker rain. If the  
14 underestimation of MPEs is such that the 3-hr rain accumulation by MPEs is  $<0.5 \text{ mm hr}^{-1}$ , then  
15 the algorithm considers it as missing rain. Such cases, indeed, exist in the data and are more  
16 frequent during the NEM than in SWM, but certainly they are not enough to explain the higher  
17 missing rain in NEM. Even if we include them as rain, the missing rain reduces only by 5%.  
18 The third aspect is higher occurrence of shallow rain. Earlier studies have shown that the rain top  
19 height is indeed low with higher occurrence of shallow rain during NEM in the study region  
20 (Saikranthi et al., 2014). It is also known from earlier studies that most of MPEs suffer in  
21 identifying the shallow rain, particularly in the vicinity of mountains (Sunilkumar et al. 2015).  
22 Therefore any of the above and or all could be the reasons for the higher occurrence of missing  
23 rain during NEM.

1 The correlation of rainfall between MPEs and reference is quite weak and insignificant at 3 hr  
2 accumulation, but improved considerably and is significant at 24-hr rain accumulation. The  
3 correlation coefficient does not show any clear seasonal difference. On the other hand, the  
4 RMSE clearly shows seasonal differences with smaller values in SWM than in NEM.  
5 Overestimation of heavy rain coupled with higher fraction of missing rain and lower fraction of  
6 POD are contributing considerably to higher RMSE in NEM. The RMSE increases with the  
7 integration time in both monsoon seasons and the daily-RMSEs are comparable in magnitude  
8 with those available in the literature (Sunilkumar et al. 2015).

9 Among different MPEs, PERSIANN appears to overdetect the rain as evidenced by larger POD  
10 and FAR and smaller missing values. However, because of its inability to detect very heavy rain  
11 ( $> 25 \text{ mm hr}^{-1}$ , not shown as a separate figure but can be seen from Figure 7) and over-detection  
12 of rain, PERSIANN produces weak correlation with the reference and large RMSE. This feature  
13 is more prominently observed during the SWM. On the other hand, TMPA performs poorly at 3-  
14 hr resolution with higher (smaller) values of misses, FAR and RMSE (POD) when compared to  
15 other MPEs. However, TMPA improves tremendously and provides much better precipitation  
16 estimates at longer temporal integration in both the monsoon seasons. Examination of detection  
17 and accuracy metrics in Table 3 reveals that CMORPH-derived precipitation estimates are the  
18 best among all MPEs at 3-hr resolution.

19 Validation of the diurnal cycle of rainfall could be more intriguing, as it is not only poorly  
20 represented by numerical models (Betts and Jakob, 2002; Nesbitt and Zipser, 2003), but also  
21 distinctly different in different seasons over the study region (Figures 4 - 6). Figure 8 shows the  
22 comparison of diurnal cycle (with 3-hr unconditional rain rate) obtained by MPEs and reference  
23 in both monsoon seasons. Clearly the diurnal cycle is quite strong during the SWM and all MPEs

1 captured the basic shape of the cycle, with nocturnal maximum and morning-noon minimum,  
2 quite well. However, all MPEs overestimate the rainfall rate, albeit with different magnitudes,  
3 almost throughout the day. The overestimation is severe (as high as a factor of 5) in the case of  
4 PERSIANN, while others show relatively small overestimations. While the amplitude of the  
5 diurnal cycle by all MPEs is nearly equal, the phase is different for different MPEs. The  
6 reference data set peaks at 15 UT (universal time = IST - 05.30), which is equivalent to 20.30  
7 IST. All MPEs capture the peak with a time lag/lead. While PERSIANN peaks 3 hours prior to  
8 the reference-peak time, others peak 3-6 hours later. It is known from earlier studies that MPEs  
9 that depend heavily on IR data shows a lagged diurnal cycle due to the lag between the detection  
10 of clouds and the occurrence of rainfall at the surface (Sorooshian et al., 2002; Janowiak et al.,  
11 2005). Though all MPEs considered here use microwave data, IR contribution appears to  
12 dominate the final rainfall product, at least in the case of PERSIANN. On the other hand, MPEs  
13 fail to reproduce the weak/insignificant diurnal cycle during the NEM. All MPEs show  
14 significant diurnal cycle, albeit with smaller amplitude than in SWM, with a broad peak centered  
15 on 15 UT. Except during the evening - midnight, the rain rates derived by MPEs and the  
16 reference agree fairly well. The overestimation of seasonal rainfall is also probably due to the  
17 overestimation of rain intensity during the evening-midnight period. The overestimation is severe  
18 in the case of PERSIANN, similar to that of in SWM.

## 19 **6. Conclusions**

20  
21 This paper describes the establishment of a dense rain gauge network, its geometric  
22 configuration and the quality assurance tests employed to generate high-quality and high-  
23 resolution rainfall data. The network consists of 36 rain gauges with an inter-gauge distance of  
24 6-12 km spread over an area of 50 km x 50 km, which makes the network much denser than the

1 operational networks in India. The locations have been chosen to have a near uniform  
2 distribution and considering several practical issues, like accessibility by road, mobile coverage  
3 for data transfer and security. The high-resolution rainfall measurements have been used to  
4 understand the small-scale variability (in space and time) in rain storms and also for validating  
5 widely used MPEs. A suite of statistical error metrics (detection and accuracy) are employed for  
6 this purpose. Important results of the analysis are summarized below.

- 7 1) Morphological features of rainfall (like spatial distribution and seasonal rain fraction) are  
8 consistent with earlier reports. Though the number of large-scale/long-lived systems  
9 (active monsoon spells) is equal in both the seasons, the average duration of each spell is  
10 larger during the SWM (6.9 days) than in NEM (4.4 days). These large-scale systems  
11 contribute more than 60% of seasonal rainfall in NEM at  $\frac{3}{4}$  of the locations in the  
12 network, whereas the contribution from small-scale/short-lived systems is found to be  
13 significant during the SWM (almost equal to that of large-scale systems). Majority of  
14 these large-scale/lon-lived systems are due to the passage of cyclones during NEM and  
15 due to propagating systems from the west coast during the active monsoon spell in SWM.
- 16 2) The cumulative distributions for rain duration and intensity (rain accumulation within the  
17 storm) show regional differences. These regional differences are more pronounced in the  
18 90<sup>th</sup> percentile of storm duration and accumulations. The western quadrants experience  
19 longer rain duration events with more rain accumulation in SWM. On the other hand,  
20 such events are seen more frequently in northern quadrants during NEM. While the  
21 number and duration of events clearly show a diurnal pattern during the SWM, such  
22 pattern is absent in NEM.

- 1        3) The diurnal cycle exhibits marked seasonal and spatial differences within the study  
2                region. The diurnal amplitudes are significant and large during the SWM, while they are  
3                insignificant at many locations and also small during the NEM. On average, the diurnal  
4                amplitudes are larger during SWM than that in NEM by a factor of  $\sim 2$ . Further, the  
5                diurnal cycle explains 70% of total variance in SWM, but only 30% in NEM. Large  
6                diurnal amplitudes are found in western quadrants during the SWM and in eastern  
7                quadrants in NEM. The propagating systems in SWM appear to be responsible for the  
8                observed late night-mid night peak. During the NEM, the rainfall occurs due to a variety  
9                of processes that either do not have any diurnal cycle or peak at different timings of the  
10               day, making the diurnal cycle weak and/or insignificant.
- 11       4) A modified exponential function has been fitted to paired correlations in both seasons for  
12               different temporal rainfall accumulations. Clearly, the correlation increases with  
13               increasing integration period up to 12 hr. However, not much improvement is seen in the  
14               correlation with further integration. The correlation falls rapidly when the high-resolution  
15               data (1 hr.) are employed for the analysis in both monsoon seasons with correlation  
16               becoming insignificant after an intergauge distance of  $\sim 30$  km. Some seasonal  
17               differences are seen in the correlation distance, but the differences are not pronounced.  
18               The scatter in the correlograms is wide spread along the fitted exponential curve for all  
19               accumulation periods in both monsoon seasons, signifying the complex variability of  
20               rainfall within the study region.
- 21       5) Comparison of cumulative distributions for MPEs and reference indicates that all MPEs  
22               severely underestimate the weak rain. The MPEs exhibit good detection skills of rain at  
23               both 3-hr and 24-hr resolutions, though considerable improvement is seen with 24-hr

1 resolution data. The FAR values validated at 24-hr resolution are nearly equal with those  
2 obtained in earlier studies with a different independent dataset (Sunilkumar et al., 2015),  
3 indicating the consistency with different datasets. The missing rain is found to be  
4 significant at higher resolution in both monsoon seasons. Though the occurrence of  
5 missing rain reduced considerably in the SWM at 24-hr resolution, such reduction is  
6 absent in NEM. Possible causes (underestimation of weaker rain and predominance of  
7 shallow rain) for the higher occurrence in NEM are examined. Among various MPEs,  
8 the performance of TMPA is found to be poor at 3-hr resolution, but improves  
9 tremendously with 24-hr integrated data. CMORPH produces best 3-hr resolution  
10 precipitation products in both monsoon seasons, as evidenced by better accuracy and  
11 detection metrics (Table 3).

- 12 6) All MPEs captured the basic shape of the diurnal cycle and the amplitude quite well  
13 during SWM, but they overestimate the rainfall throughout the day. They fail to  
14 reproduce the insignificant diurnal cycle during NEM, rather MPEs show a significant  
15 diurnal cycle in NEM, albeit with a relatively smaller amplitude.

16 Acknowledgments: The authors thank various data providers for generating and making it  
17 available for research.

18

19

20

21

1 References

- 2 Adler, R. F., Kidd, C., Petty, G., Morissey, M., and Goodman, H. M.: Intercomparison of global  
3 precipitation products: The third precipitation intercomparison project (PIP3), *Bull. Amer.*  
4 *Meteor. Soc.*, 82, 1377-1396, 2001.
- 5 Anderson, T. W.: *The Statistical Analysis of Time Series*, 704 pp., John Wiley, Hoboken, N.J.,  
6 1971.
- 7 Aonashi, K., Awaka, J., Hirose, M., Kozu, T., Kubota, T., Liu, G., Shige, S., Kida, S., Seto, S.,  
8 Takahashi, N., and Takayabu, Y. N.: GSMaP passive microwave precipitation retrieval  
9 algorithms: Algorithm description and validation, *J. Meteor. Soc. Japan*, 87A, 119-136, 2009.
- 10 Baigorria, A., Jones, J. W., and O'Brien, J. J.: Understanding rainfall spatially variability in  
11 southeast USA at different time scales, *Int. J. Climatol.*, 27, 749-760, 2007.
- 12 Betts, A. K., and Jacob, C.: Study of diurnal cycle of convective precipitation over Amazonia  
13 using a single column model, *J. Geophys. Res.*, 107, 4732, doi: 10.1029/2002JD002264, 2002.
- 14 Bras, R. L., and Rodriguez-Iturbe, I.: *Random functions and Hydrology*, PP 559, Mineola,  
15 Dover, New York, 1993.
- 16 Chen, Y., Liu, H., An, J., Gorsdorf, U., and Berger, F. H.: A field experiment on the small scale  
17 variability of rainfall based on a network of micro rain radars and rain gauges, *J. Appl. Meteor.*  
18 *Climatol.*, 54, 243-255, 2015.
- 19 Ciach, G. J., and Krajewski, W. F.: Analysis and modelling of spatial correlation in small scale  
20 rainfall in Central Oklahoma, *Ad. Water Resour.*, 29, 1450-1463, 2006.

1 Dee, D. P., et al.: The ERA-Interim reanalysis: configuration and performance of the data  
2 assimilation system, *Quart. J. Royal Meteorol. Soc.*, 137, 553-597, 2011.

3 Dinku, T., Connor, S. J., Ceccato, P.: Comparison of CMORPH and TRMM – 3B42 over  
4 mountainous regions of Africa and South America, in: *Satellite Rainfall Applications for surface*  
5 *Hydrology*, Springer, Netherlands, 193-204, 2010.

6 Dzotsi, K. A., Matyas, C. J., Jones, J. W., Baigorria, G., and Hoogenboom, G.: Understanding  
7 high resolution space-time variability of rainfall in southwest Georgia, United States, *Int. J.*  
8 *Climatol.*, 34, 3188-3203, 2014.

9 Ebert, E., Janowiak, J., and Kidd, C.: Comparison of near real time precipitation estimates from  
10 satellite observations and numerical models, *Bull. Amer. Meteorol. Soc.*, 88, 47-64, 2007.

11 Ghajarnia, N., Liaghat, A., and Arsteh, P. D.: Comparison and evaluation of high resolution  
12 estimation products in Urmia basin-Iran, *Atmos. Res.*, 158-159, 50-65, 2015.

13 Habib, E., Krajewski, F., and Ciach, G. J.: Estimation of rainfall interstation correlation, *J.*  
14 *Hydrometeorol.*, 2, 621-629, 2001.

15 Habib, E., Haile, A., Tian, Y., and Joyce, R. J.: Evaluation of the high-resolution CMORPH  
16 satellite rainfall product using dense rain gauge observations and radar-based estimates, *J.*  
17 *Hydrometeorol.*, 13, 1784-1798, 2012.

18 Habib, E., Henschke, A., and Adler, R. F.: Evaluation of TMPA satellite-based research and real-  
19 time rainfall estimates during six tropical –related heavy rainfall events over Louisiana, USA,  
20 *Atmos. Res.*, 3, 373-388, 2009.

1 Houze Jr, R. A., Wilton, D. C., and Smull, B. F.: Monsoon convection in the Himalayan region  
2 as seen by the TRMM precipitation radar, *Q. J. R. Meteorol. Soc.*, 133, 1389-1411, 2007.

3 Hsu, K. L., Gao, X., Sorooshian, S., and Gupta, H. V.: Precipitation estimation from remotely  
4 sensed information using artificial neural networks, *J. Appl. Meteorol.*, 36, 1176-1190, 1997.

5 Huffman, G. J., Adler, R. F., Bolvin, D. T., Gu, G., Nelkin, E. J., Bowman, K. P., Hong, Y.,  
6 Stocker, E. F., and Wolf, D. B.: The TRMM multi satellite precipitation analysis (TMPA): quasi  
7 global, multiyear, combined sensor precipitation estimates at finer scales, *J. Hydrometeorol.*, 8,  
8 38-55, 2007.

9 Janowiak, J. E., Kousky, V. E., and Joyce, R. J.: Diurnal cycle of precipitation determined from  
10 the CMORPH high spatial and temporal resolution global precipitation analyses, *J. Geophys.*  
11 *Res.*, 110, D23105, doi: 1029/2005JD006156, 2005.

12 Joyce, R. J., Janowiak, J., Arkin, P., and Xie, P.: CMORPH: A method that produces global  
13 precipitation estimates from passive microwave and infrared data at high spatial and temporal  
14 resolutions, *J. Hydrometeorol.*, 5, 487-503, 2004.

15 Kidd, C., Bauer, P., Turk, J., Huffman, G. J., Joyce, R., Hsu, K. L., and Braithwaite, D.:  
16 Intercomparison of high-resolution precipitation products over Northwest Europe, *J.*  
17 *Hydrometeorol.*, 13, 67-83, 2012.

18 Kidd, C., Levizzani, V., Turk, J., and Ferraro, R.: Satellite precipitation measurements for water  
19 resources monitoring, *J. Amer. Water Resour. Assoc.*, 45, 567-579, 2009.

20 Kikuchi, K., and Wang, B.: Diurnal precipitation regimes in the global tropics, *J. Climate*, 21,  
21 2680-2696, 2008.

1 Krajewski, W. F., Ciach, G. J., and Habib, E.: An analysis of small scale variability in different  
2 climatic regimes, *Hydrol. Sci. J.*, 48, 151-162, 2003.

3 Kubota, T., Shinge, S., Hashizume, H., Aonashi, K., Takahashi, N., Seto, S., Hirose, M.,  
4 Takayabu, Y. N., Nakagawa, K., Iwaanami, K., Ushio, T., Kachi, M., and Okamoto, K.: Global  
5 Precipitation Map using Satellite borne Microwave Radiometers by the GSMaP Project:  
6 Production and validation, *IEEE Trans. Geosci. Remote Sens.*, 45, 2259-2275, 2007.

7 Kucera, P. A., Ebert, E. E., Turk, F. J., Levizzani, V., Kirschbaum, D., Tapiador, F. J., Loew, A.,  
8 and Borsche, M.: Precipitation from space advancing earth system science, *Bull. Amer.*  
9 *Meteorol. Soc.*, 365-375, doi:10.1175/BAMS-D-11-00171.1, 2013

10 Levizzani, V., Bauer, P., and Turk, F. J.: *Measuring precipitation from space*, Springer,  
11 Netherlands, 722 pp., doi:10.1007/978-1-4020-5835-6, 2007

12 Li, L., Hong, Y., Wang, J., Adler, R. F., Policelli, F. S., Habib, S., Irwn, D., Korme, T., and  
13 Okello, L.: Evaluation of the real-time TRMM –based multi-satellite precipitation analysis for an  
14 operational flood prediction systems in Nzoia basin, Lake Victoria, Africa, *Nat. Hazards*, 50,  
15 109-123, 2009.

16 Li, Z., Yang, D., Hong, Y., Zhang, J., and Qi, Y.: Characterizing spatiotemporal variations of  
17 hourly rainfall by gauge and radar in the mountainous three Gorges region, *J. Appl. Meteor.*  
18 *Climatol.*, 53, 873-889, 2014.

19 Liechti, T. C., Matos, J. P., Boillat, J.-L., and Schleiss, A. J.: Comparison and evaluation of  
20 satellite derived precipitation products for hydrological modeling of the Zambezi river basin,  
21 *Hydrol. Earth Syst. Sci.*, 16, 489-500, 2012.

- 1 Luini, L., and Capsoni, C.: The impact of space and time averaging on the spatial correlation of  
2 rainfall, *Radio Sci.*, 47, RS3013, doi: 10.1029/2011RS004915, 2012.
- 3 Mandapaka, P. V., and Qin, X.: Analysis and characterization of probability distribution and  
4 small scale variability of rainfall in Singapore using a dense gauge network, *J. Appl. Meteor.*  
5 *Climatol.*, 52, 2781-2796, 2013.
- 6 Mehran, A., and AghaKouchak, A.: Capabilities of satellite precipitation datasets to estimate  
7 heavy precipitation rates at different temporal accumulations, *Hydro. Proc.*, 28, 2262-2270,  
8 2014.
- 9 Mohan, T.: Characteristics of wet and dry spells during southwest monsoon season over  
10 southeast India-a diagnostic study, Dept. of Meteorology and oceanography, Andhra University,  
11 Visakhapatnam, India, 2011.
- 12 Nesbitt, S. W., and Zipser, E. J.: The diurnal cycle of rainfall and convective intensity according  
13 to three years of TRMM measurements, *J. Climate*, 16, 1456-1475, 2003.
- 14 Prakash, S., Sathiyamoorthy, V., Mahesh, C., and Gairola, R. M.: An evaluation of high-  
15 resolution multisatellite products over the Indian monsoon region, *Int. J. Remote Sens.*, 35,  
16 3018-3035, 2014.
- 17 Prat, O. P., and Nelson B. R.: Evaluation of precipitation estimates over CONUS derived from  
18 satellite, radar, and rain gauge data sets at daily to annual scales (2002-2012), *Hydrol. Earth.*  
19 *Syst. Sci.*, 19, 2037-2056, 2015.

1 Radhakrishna, B., Rao, T. N., Rao, D. N., Rao, N. P., Nakamura, K., and Sharma, A. K.: Spatial  
2 and seasonal variability of raindrop size distributions in southeast India, *J. Geophys. Res.*, 114,  
3 D04203, doi:10.1029/2008JD011226, 2008.

4 Rahman, S. H., Sengupta, D., and Ravichandran . M.: Variability of Indian summer monsoon  
5 rainfall in daily data from gauge and satellite, *J. Geophys. Res.*, 114, D17113, doi:  
6 10.1029/2008JD011694, 2009.

7 Rajeevan, M., Bhate, J., Kale, K. D., and Lal, B.: High resolution daily gridded rainfall data for  
8 the Indian region: Analysis of break and active monsoon spells, *Curr. Sci.*, 91, 296-306, 2006.

9 Raju, G.: Engineering challenges in the Megha-Tropiques satellite, *Cur. Sci.*, 104, 1662-1670,  
10 2013.

11 Rao, T. N., Rao, D. N., Mohan, K., Raghavan, S.: Classification of tropical precipitating systems  
12 and associated Z-R relationships, *J. Geophys. Res.*, 106, 17699-17712, 2001.

13 Rao, T. N., Radhakrishna, B., Nakamura, K., and Prabhakara Rao, N.: Differences in raindrop  
14 size distribution from southwest monsoon to northeast monsoon at Gadanki, *Q. J. R. Meterol.*  
15 *Sci.*, 135, 1630-1637, 2009.

16 Roca, R., Brogniez, H., Chambon, P., Chomette, O., Cloche, S., Gosset, M. E., Mahfouf, J-F.,  
17 Raberanto P., and Viltard, N.: The Megha-Tropiques mission: a review after three years in orbit,  
18 *Front. Earth Sci.*, 3, doi:10.3389/feart.2015.00017, 2015

19 Saikranthi, K., Rao, T. N., Radhakrishna, B., and Rao, S. V. B.: Morphology of the vertical  
20 structure of precipitation over India and adjoining oceans based on the long-term measurements  
21 of TRMM PR, *J. Geophys. Res.*, 119, 8433-8449, 2014.

1 Sapiano, M. R. P., and Arkin, P. A.: An intercomparison and validation of high-resolution  
2 satellite precipitation estimates with 3-hourly gauge data, *J. Hydrometeorol.*, 10, 149-166, 2009.

3 Simpson, M., Warrior, H., Raman, S., Aswathanarayana P. A., Mohanty, U. C., and Suresh. R.:  
4 Sea breeze Initiated Rainfall over the East Coast of India during the Indian Southwest Monsoon,  
5 *Natural Hazards*, 42, 401-413, 2007.

6 Sohn, B. J., Jin-Han, H., and Seo, E.: Validation of satellite-based high resolution rainfall over  
7 the Korean Peninsula using data from a dense rain gauge network, *J. Appl. Meteor. Climatol.*,  
8 49, 701-714, 2010.

9 Sorooshian, S., Gao, X., Hsu, K., MADDUX, R. A., Hong, Y., Gupta, H. V., and Imam, B.:  
10 Diurnal variability of tropical rainfall retrieved from combined GOES and TRMM satellite  
11 information, *J. Climate*, 15, 983-1001, 2002.

12 Sorooshian, S., Hsu, K., Gao, X., Gupta, H. V., Imam, B., and Braithwaite, D.: Evaluation of  
13 PERSIANN system satellite-based estimates of tropical rainfall. *Bull. Amer. Meteorol. Soc.*, 81,  
14 2035-2046, 2000.

15 Sunilkumar, K., Rao, T. N., Saikranthi, K., and Rao, M. P.: Comprehensive evaluation of  
16 multisatellite precipitation estimates over India using high-resolution gridded rainfall data, *J.*  
17 *Geophys. Res.*, 120, 8987-9005, doi: 10.1002/2015JD023437, 2015. Tian, Y., Lidard, C. D. P.,  
18 Choudhury, C. B. J., and Garcia, M.: Multitemporal analysis of TRMM-based satellite  
19 precipitation products for land data assimilation application, *J. Hydrometeorol.*, 8, 1165-1183,  
20 2007.

1 Tokay, A., and Ozturk, K.: An experimental study of spatial variability of rainfall, J.  
2 Hydrometeorol., 15, 801-812, 2012.

3 Tokay, A., Roche R. J., and Bashor, P. J.: An experimental study of the small-scale variability of  
4 rainfall, J. Hydrometeorol., 13, 351-365, 2014.

5 Turk, F. J., Arkin, P., Sapiano, M. R. P., and Ebert, E. E.: Evaluating high-resolution  
6 precipitation products, Bull. Amer. Meteor. Soc., 89, 1911-1916, 2008.

7 Uma, R., Kumar, T. V. L., Narayanan, M. S., Rajeevan, M., Bhate, J., and Niranjan Kumar, K.:  
8 Large scale features and assessment of spatial scale correspondence between TMPA and IMD  
9 rainfall datasets over Indian landmass, J. Earth syst. Sci., 122, 573-588, 2013.

10 Villarini, G., Mandapaka, P. V., Krajewski, W. F., and Moore, R. J.: Rainfall and sampling  
11 uncertainties: A rain gauge perspective, J. Geophys. Res., 113, D11102,  
12 doi:10.1029/2007JD009214, 2008.

13 Nešpor, V., and Sevruk, B.: Estimation of wind-induced error of rainfall gauge measurements  
14 using a numerical simulation, J. Atmos. Oceanic Tech., 16, 450-464, 1999.

15 Wang, N-Y., Liu, C., Ferraro, R., Wolff, D., Zipser Ed., Kummerow, C., TRMM 2A12 land  
16 precipitation product – status and future plans, J. Meteorol. Soc. Japan., 87A, 237-253, 2009.

17 Weisman, M. L., and Rotunno, R.: A theory for strong long-lived squall lines revisited. J. Atmos.  
18 Sci., 61, 361-382, 2004.

19 World Meteorological Organization: Guide to meteorological instruments and methods of  
20 observation, WMO-No.8, Seventh edition, Geneva, 2008

1 Yang, S., and Smith, E. A.: Mechanisms for diurnal variability of global tropical rainfall  
2 observed from TRMM, *J. Climate*, 19, 5190-5226. 2006.

3 Zängl, G.: Interaction between dynamics and cloud microphysics in orographic precipitation  
4 enhancement: A modelling study of two North Alapine heavy –precipitation events, *Mon. Wea.*  
5 *Rev.*, 135, 2817-2840, 2007.

6

7

8

9

10

11

12

13

14

15

16

17

18

1 Figure captions

2 Figure 1: Spatial distribution of mean seasonal rainfall (shading) and wind pattern (arrows) on  
3 850 hPa level during (a) SWM and (b) NEM. Note that the scales are different for SWM and  
4 NEM. The black solid contour line covering the north and central India indicates the monsoon  
5 trough. The red colored square box in Figure (a) indicates the region of rain gauges. (c)  
6 Location of rain gauges in the network (indicated with stars). The shading represents the  
7 topography (m). The region is divided into 4 quadrants and each quadrant is numbered as 1, 2, 3  
8 and 4. The data in dashed box are used for the evaluation of MPEs. (d) The ratio of measured  
9 and reference (calibrator – Young 52 260) values at 3 rain rates are shown for each rain gauge  
10 location, illustrating the data quality by each gauge.

11 Figure 2: Spatial distribution of average seasonal rainfall for (a) SWM and (b) NEM. Also  
12 overlaid is the location of rain gauges.

13 Figure 3: Cumulative distributions for event duration and rain accumulation within the event in 4  
14 quadrants (color-coded) of the study region during (a) SWM and (b) NEM, depicting the  
15 regional variability in rain events.

16 Figure 4: Diurnal variation of event duration and rain accumulation in 4 quadrants of the study  
17 region during (a) SWM and (b) NEM. Accumulated rain (in mm) is shown in the color bar.

18 Figure 5: Diurnal variation of rainfall at all rain gauge locations during (a) SWM and (b) NEM.  
19 The vector length and pointing arrows indicate the amplitude and phase (peak rainfall hour),  
20 respectively, of the first harmonic. The shading and blue arrows indicate, respectively,  
21 topography and insignificant diurnal amplitudes. c) Percentage contribution of variance by first  
22 harmonic to the total variance at each rain gauge location during both monsoons.

1 Figure 6: Correlograms (correlation coefficient vs. intergauge distance) for 1 hr, 3 hr, 12 hr and  
2 24 hr rain accumulations during (a) SWM and (b) NEM. The red curve indicates the fitted  
3 modified exponential function to the data. The accumulation period, slope of the curve and  
4 spatial correlation distance are also shown in each plot.

5 Figure 7: Cumulative distributions of rain rate (mm/3hr) for various MPEs (color-coded) and  
6 rain gauge network at (13.375° N, 79.125° E) (black curve) during (a) SWM and (b) NEM.

7 Figure 8: Comparison of diurnal variation of rainfall obtained by various MPEs and reference  
8 data set (rain gauge network) during (a) SWM and (b) NEM. The rain gauge data are integrated  
9 to match with the timings of MPE. Note that the time is given in universal time (UT).

10 Table captions:

11 Table 1: Table 1: Description of MPEs used in the present study, their data availability, spatial  
12 and temporal resolutions and input data used to generate the MPE with relevant references.

13 Table 2: Statistics of rain storms in each quadrant during SWM and NEM. The statistics include  
14 the number of storms and mean, IQR, 90<sup>th</sup> percentile and maximum values for storm duration  
15 and accumulated rain within the storm.

16 Table 3: Table 3: Comparison of high-resolution MPEs with reference data in terms of detection  
17 (POD, MIS and FAR) and accuracy (RMSE and Correlation coefficient) metrics. The  
18 comparison has been made at two temporal integrations, 3 hr (first value) and 24 hr (second  
19 value).

20

21



Table 1: Description of MPEs used in the present study, their data availability, spatial and temporal resolutions and input data used to generate the MPE with relevant references.

<b>Name of MPE (reference)</b>	<b>Data availability</b>	<b>Spatial and Temporal resolution</b>	<b>Basic input sensors data</b>	<b>Data accessibility and Technical documentation</b>
CMORPH (Joyce <i>et al</i> 2004)	1998 - Till date	0.25°×0.25°, 3 hourly	PMW from DMSP 13,14&15(SSM/I), NOAA-25,16,17&18 (AMSU-B),AMSR-E and TMI,IR motion vectors form geostationary satellite	<a href="http://ftp.cpc.ncep.noaa.gov/precip/CMORPH_V1.0/RAW/0.25deg-3HLY/">http://ftp.cpc.ncep.noaa.gov/precip/CMORPH_V1.0/RAW/0.25deg-3HLY/</a>
GSMaP (Okamoto <i>et al</i> 2005)	2010 - Till date	0.1°×0.1°, Hourly	GPM-core GMI,TRMM TMI, GCOM-W1 AMSR2, DMSP SSMIs, NOAA AMSU, MetOp series AMSU, and geostationary IR developed by GsMAP project.	<a href="ftp://hokusai.eorc.jaxa.jp/">ftp://hokusai.eorc.jaxa.jp/</a>
PERSIANN (Hsu <i>et al</i> 1997)	1997 - Till date	0.25°×0.25°, 3 hourly	IR from GOES-8,10, GMS-5, METEOSAT - 6, 7 and PMW from TRMM,NOAA AND DMSP	<a href="http://chrs.web.uci.edu/persiann/data.html">http://chrs.web.uci.edu/persiann/data.html</a>
TRMM 3B42 (Huffman <i>et al</i> 2007)	1997 - Till date	0.25°×0.25°, 3 hourly	TMI,AMSR-E,SSM/I,AMSU,MHS and microwave adjusted merged geo infrared (IR)	<a href="http://mirador.gsfc.nasa.gov/">http://mirador.gsfc.nasa.gov/</a>

Table 2: Statistics of rain storms in each quadrant during SWM and NEM. The statistics include the number of storms and mean, IQR, 90<sup>th</sup> percentile and maximum values for storm duration and accumulated rain within the storm.

<b>Region/ Season</b>	<b>No. of Events</b>	<b>Rain duration (min)</b>				<b>Accumulated rainfall (mm)</b>			
		<b>Mean</b>	<b>IQR</b>	<b>90<sup>th</sup></b>	<b>Max</b>	<b>Mean</b>	<b>IQR</b>	<b>90%</b>	<b>Max</b>
<b><u>SWM</u></b>									
<b>1</b>	674	64.5	55	169	456	6.58	6.2	17.4	70.8
<b>2</b>	792	55.3	47	123	423	6.04	5.6	16	81
<b>3</b>	774	70.1	52	193	592	6.65	6.5	17.8	76
<b>4</b>	670	58	47	133	462	5.83	4.6	14.2	86.4
<b><u>NEM</u></b>									
<b>1</b>	549	65.6	55	167	656	6.55	6.2	19.6	79.8
<b>2</b>	746	67.1	55	167	478	7.26	6.2	18.8	126
<b>3</b>	565	60.2	56	140	521	5.76	5.2	14.6	65.4
<b>4</b>	514	68	58	138	1425	6.02	5.1	14.4	99.6

Table 3: Comparison of high-resolution MPEs with reference data in terms of detection (POD, MIS and FAR) and accuracy (RMSE and Correlation coefficient) metrics. The comparison has been made at two temporal integrations, 3 hr (first value) and 24 hr (second value).

	SWM				NEM			
	CMORPH	GSMaP	TMPA	PERSIANN	CMORPH	GSMaP	TMPA	PERSIANN
<b>RMSE</b>	3.9, 7.8	4.4, 9.4	5.1, 7.7	4.1, 9.5	5.5, 13.8	6, 16.6	6.2, 10.2	5.4, 12.2
<b>CORR.</b>	0.4, 0.6	0.1, 0.3	0.2, 0.6	0.1, 0.3	0.3, 0.4	0.2, 0.5	0.3, 0.6	0.1, 0.5
<b>FAR</b>	8.3, 18.8	10.8, 24.4	8.2, 24.4	16.5, 46.1	3.6, 1.6	5.2, 7.2	2.9, 2.4	7, 12
<b>MIS</b>	32, 18.8	46.6, 18.8	50, 17.8	47.7, 13.8	42.5, 38.3	49.2, 38.3	53.3, 31.6	45, 40
<b>POD</b>	67.9, 81.8	53.3, 81.8	50.8, 82.1	52.2, 86.1	56.6, 61.6	50.8, 61.6	46.6, 68.3	55, 60

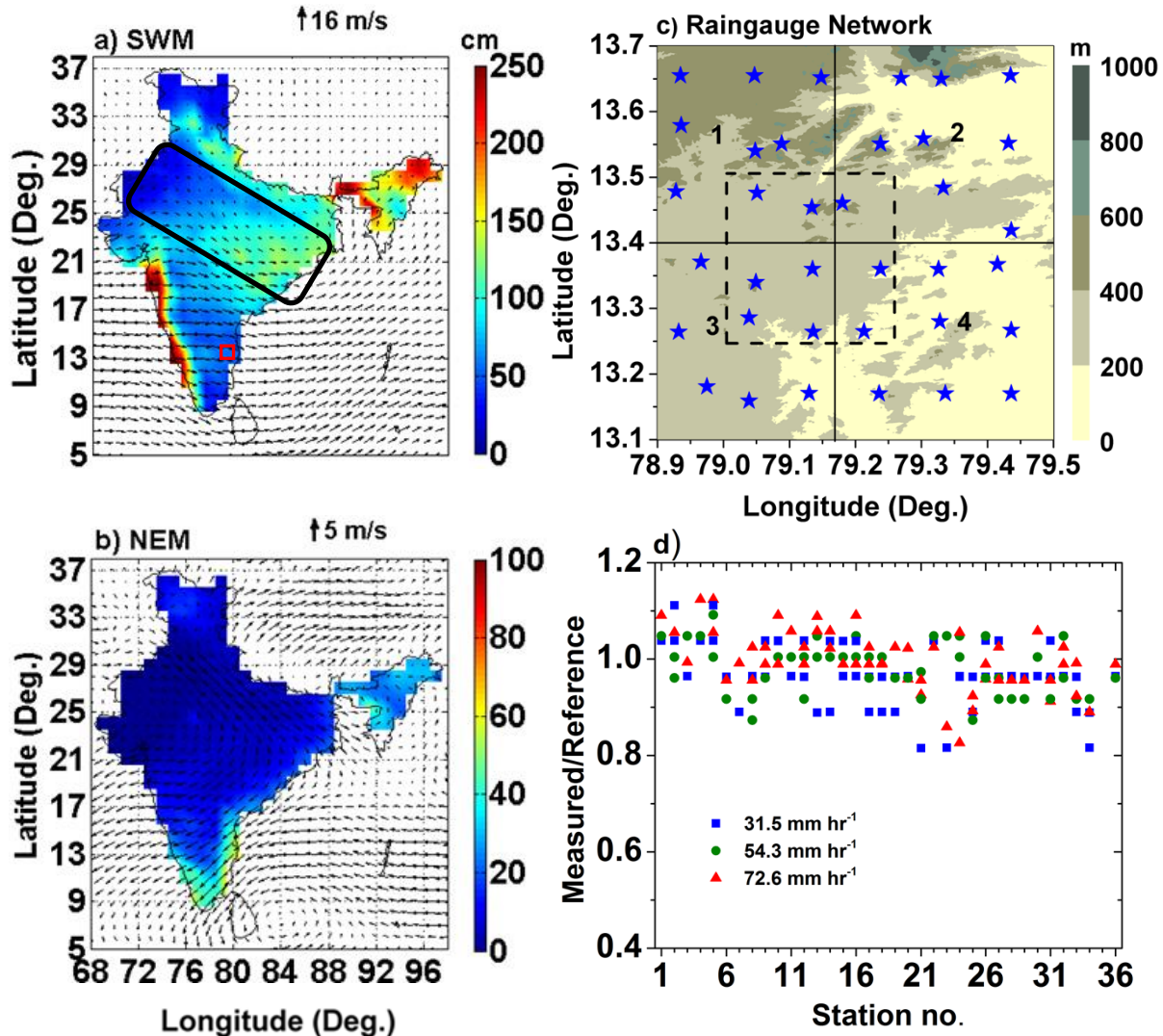


Figure 1: Spatial distribution of mean seasonal rainfall (shading) and wind pattern (arrows) on 850 hPa level during (a) SWM and (b) NEM. Note that the scales are different for SWM and NEM. The black solid contour line covering the north and central India indicates the monsoon trough. The red colored square box in Figure (a) indicates the region of rain gauges. (c) Location of rain gauges in the network (indicated with stars). The shading represents the topography (m). The region is divided into 4 quadrants and each quadrant is numbered as 1, 2, 3 and 4. The data in dashed box are used for the evaluation of MPEs. (d) The ratio of measured and reference (calibrator – Young 52 260) values at 3 rain rates are shown for each rain gauge location, illustrating the data quality by each gauge.

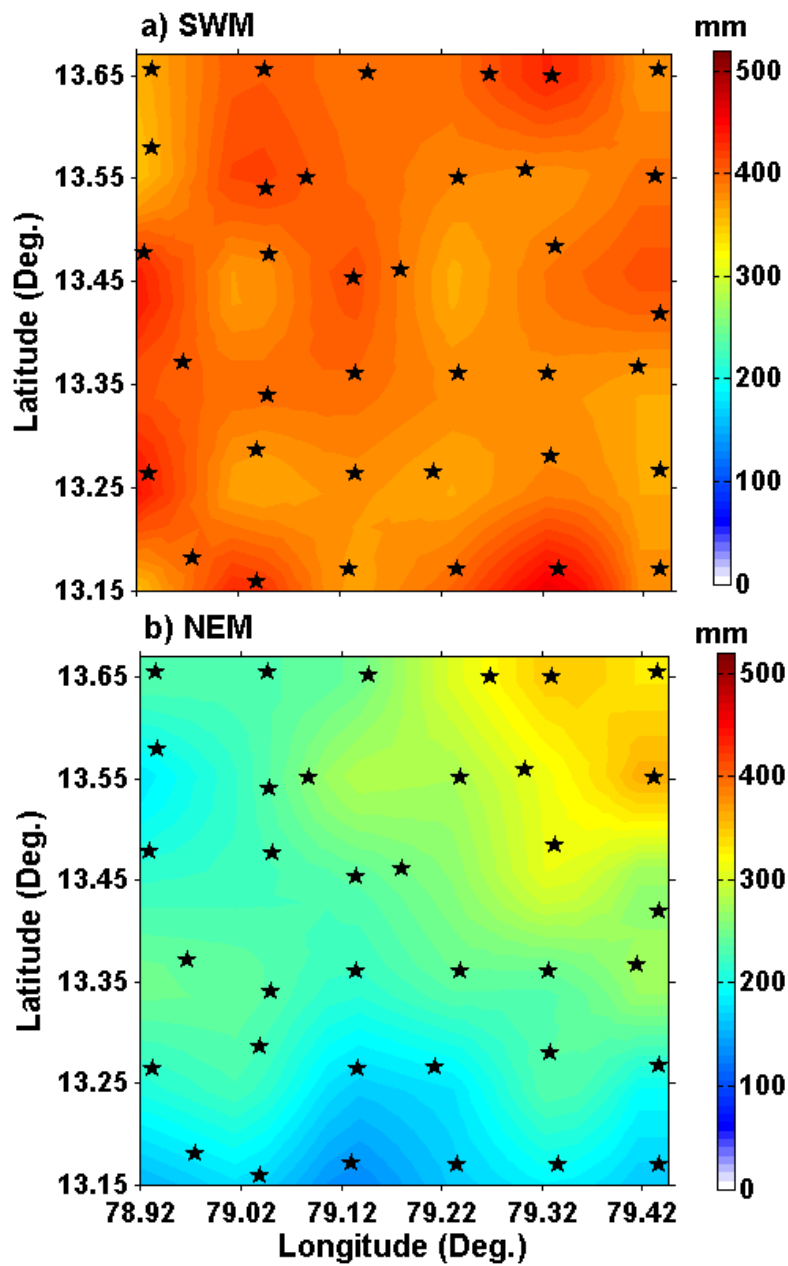


Figure 2: Spatial distribution of average seasonal rainfall for (a) SWM and (b) NEM. Also overlaid is the location of rain gauges.

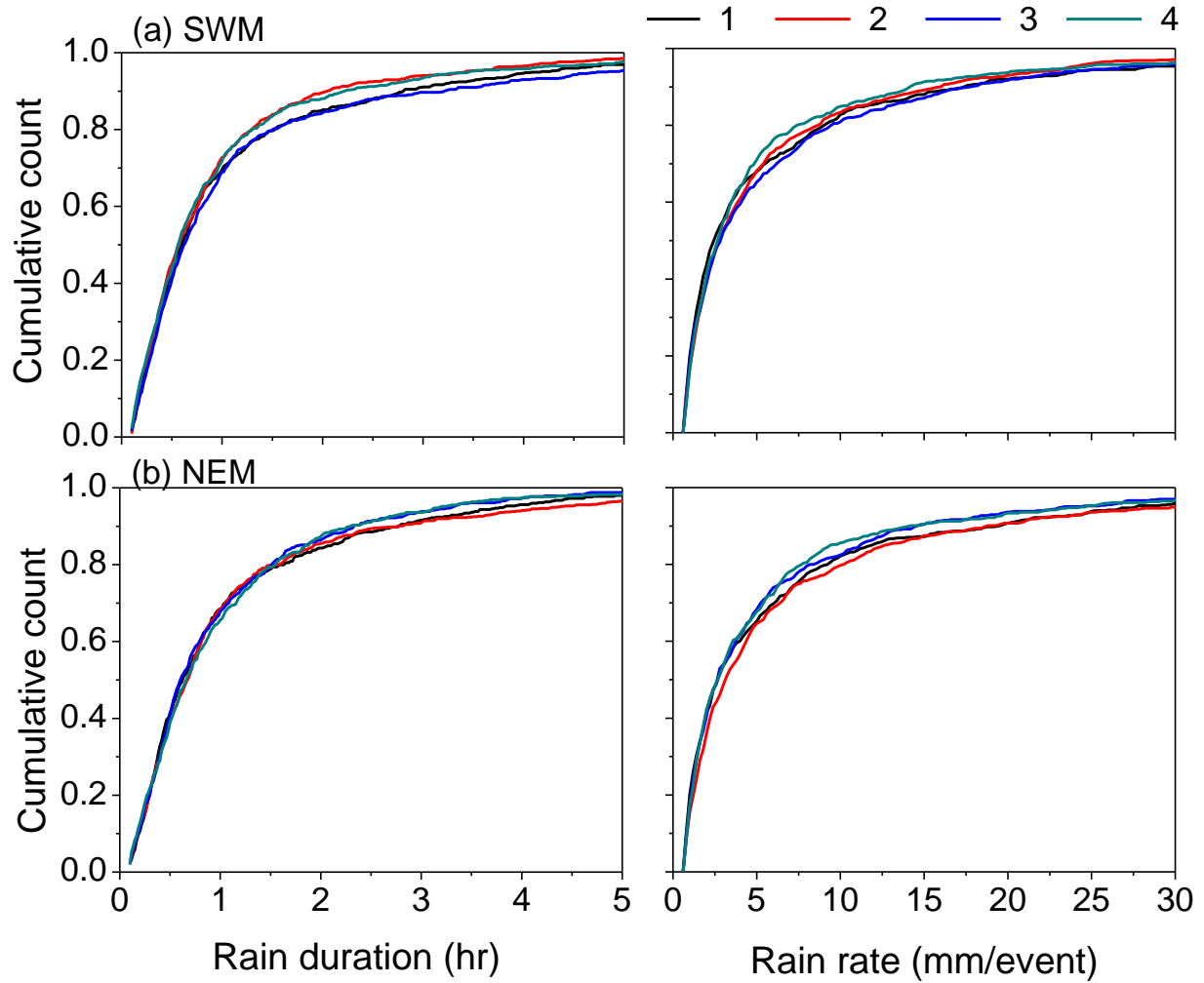


Figure 3: Cumulative distributions for event duration and rain accumulation within the event in 4 quadrants (color-coded) of the study region during (a) SWM and (b) NEM, depicting the regional variability in rain events.

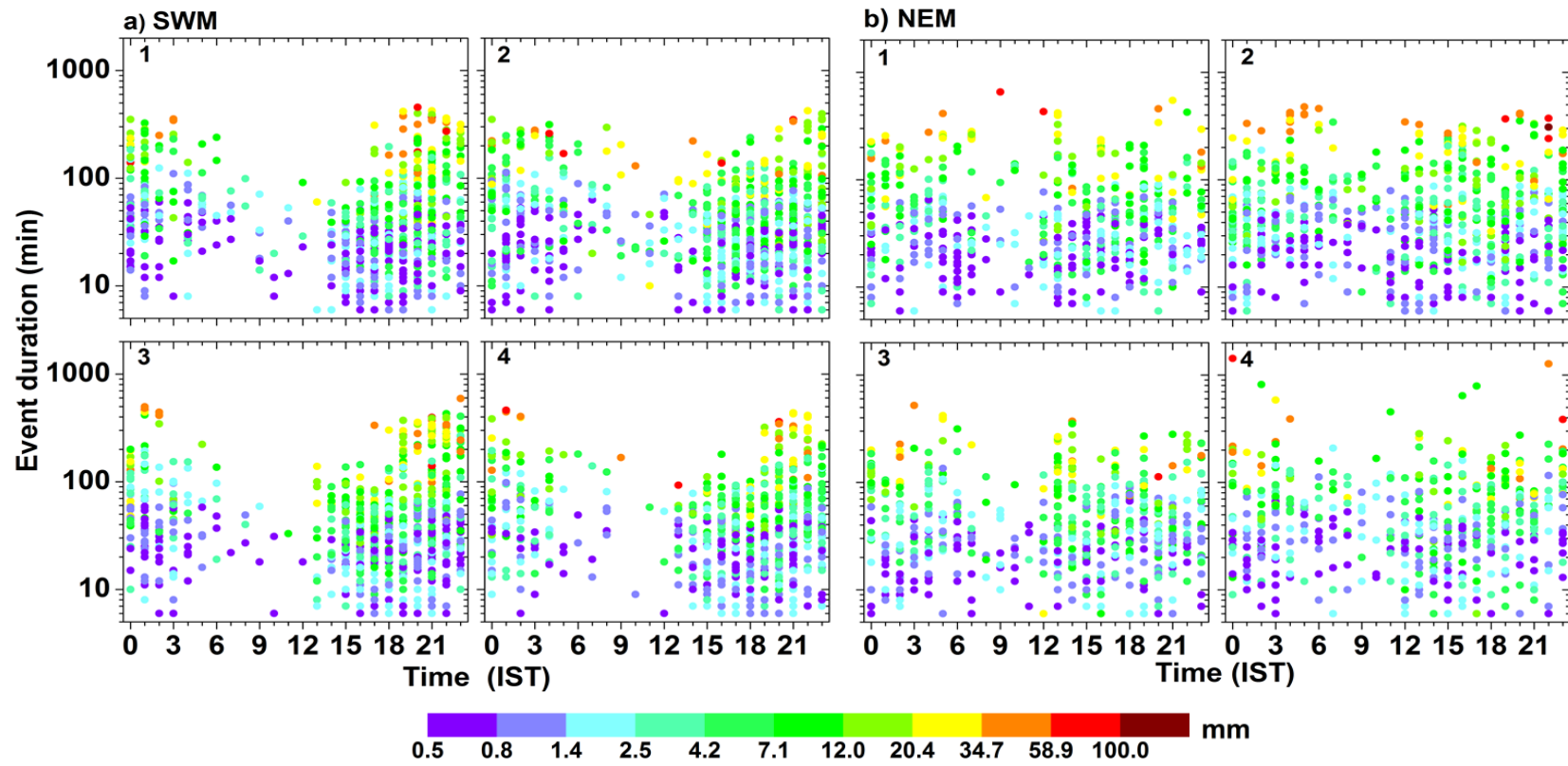


Figure 4: Diurnal variation of event duration and rain accumulation in 4 quadrants of the study region during (a) SWM and (b) NEM. Accumulated rain (in mm) is shown in the color bar.

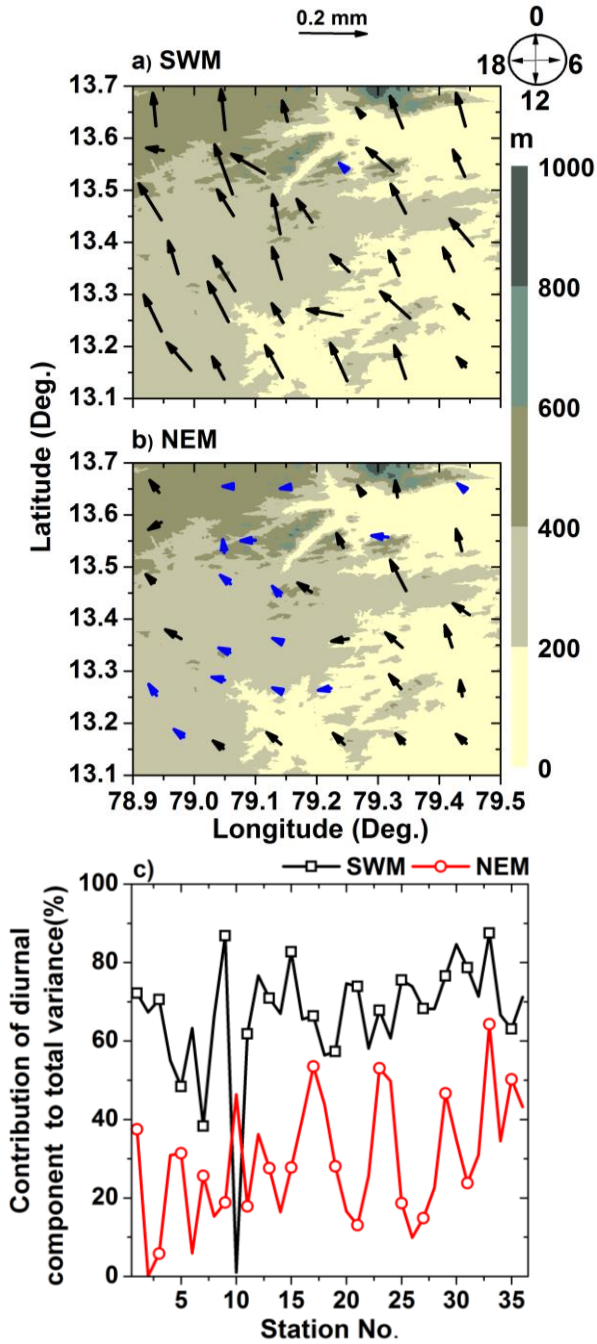


Figure 5: Diurnal variation of rainfall at all rain gauge locations during (a) SWM and (b) NEM.

The vector length and pointing arrows indicate the amplitude and phase (peak rainfall hour), respectively, of the first harmonic. The shading and blue arrows indicate, respectively, topography and insignificant diurnal amplitudes. c) Percentage contribution of variance by first harmonic to the total variance at each rain gauge location during both monsoons.

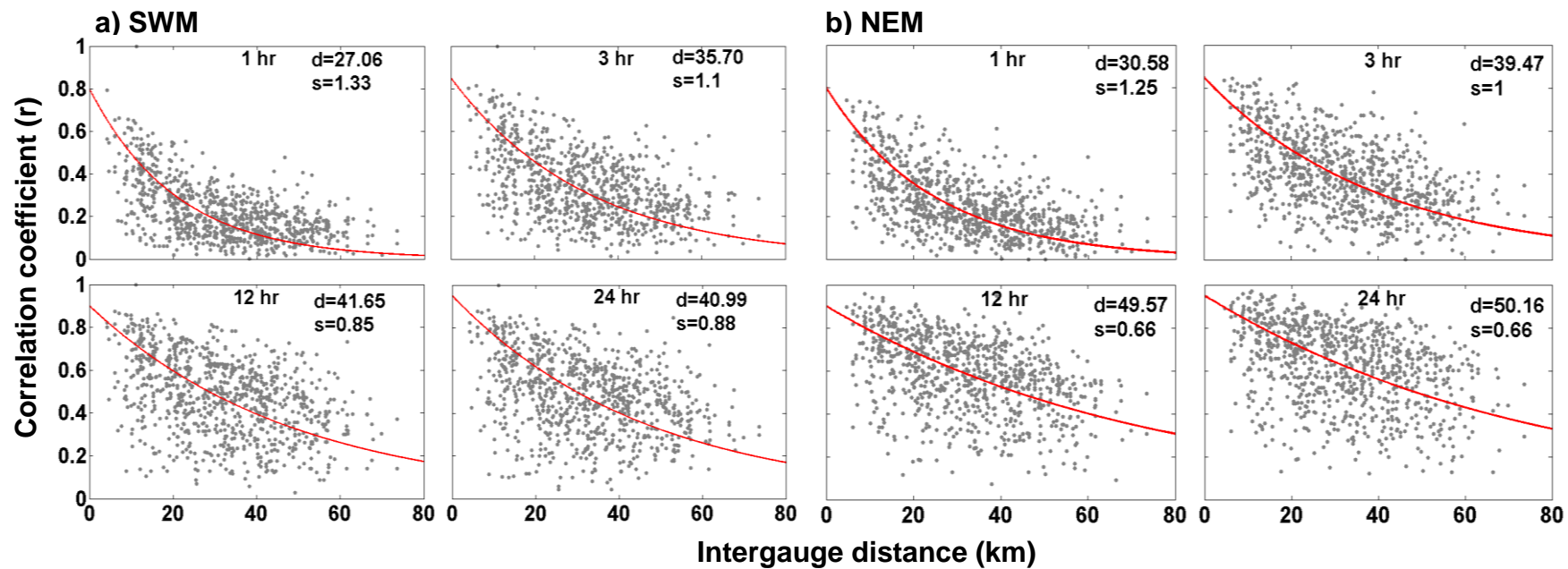


Figure 6: Correlograms (correlation coefficient vs. intergauge distance) for 1 hr, 3 hr, 12 hr and 24 hr rain accumulations during (a) SWM and (b) NEM. The red curve indicates the fitted modified exponential function to the data. The accumulation period, slope of the curve and spatial correlation distance are also shown in each plot.

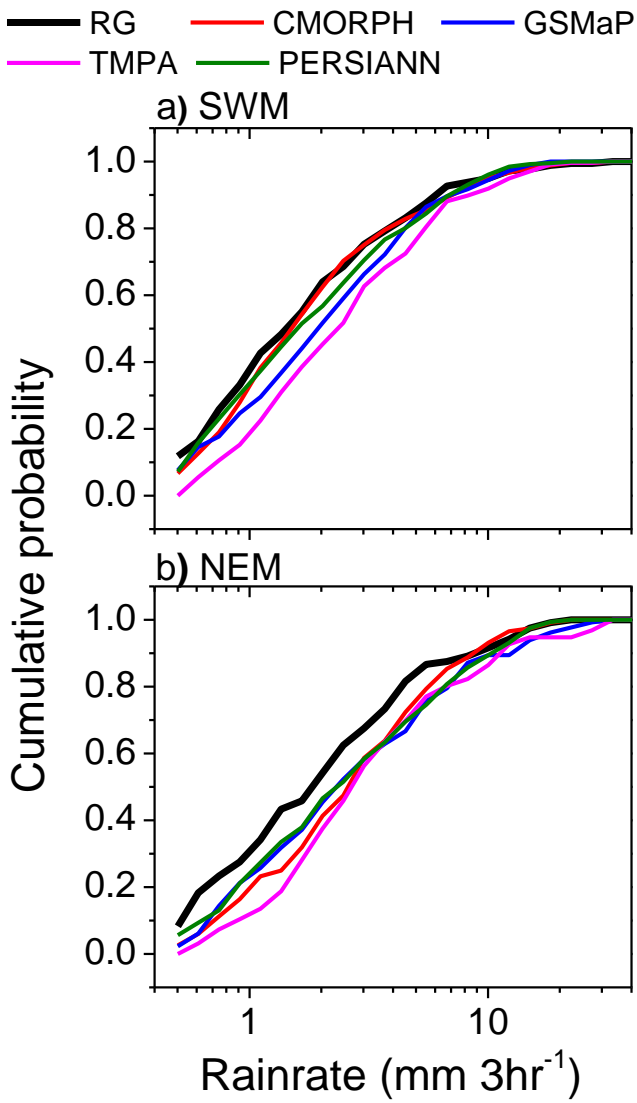


Figure 7: Cumulative distributions of rain rate (mm/3hr) for various MPEs (color-coded) and rain gauge network at (13.375° N, 79.125° E) during (a) SWM and (b) NEM.

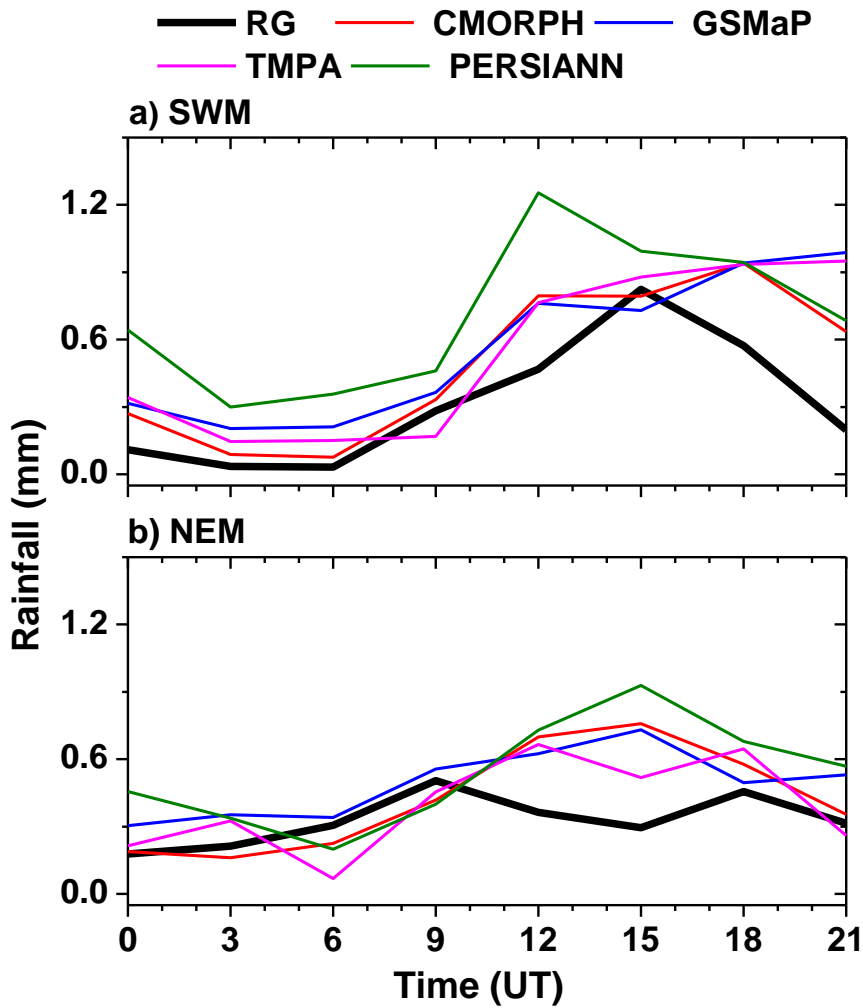


Figure 8: Comparison of diurnal variation of rainfall obtained by various MPEs and reference data set (rain gauge network) during (a) SWM and (b) NEM. The rain gauge data are integrated to match with the timings of MPE. Note that the time is given in universal time (UT).